Incorporating plant access to groundwater in existing global, satellite-based evaporation estimates

P. Hulsman[1], J. Keune[1], A. Koppa[1], J. Schellekens[2], D. G. Miralles[1]

[1]Hydro-Climate Extremes Lab (H-CEL), Ghent University, Ghent, Belgium
[1]Planet, Haarlem, Netherlands

Key Points:

- Plant access to groundwater is often ignored in global evaporation estimates, yet it can be crucial during dry conditions.
- A new, conceptual approach to incorporate groundwater-sourced evaporation in existing global, satellite-based models is presented.
- Considering groundwater affects the dynamics of evaporation in 22% of the continental surface and increases global land evaporation by 0.5%.

Corresponding author: Petra Hulsman, `Petra.Hulsman@ugent.be`

Abstract

Groundwater is an important water source for evaporation, especially during dry conditions. Despite this recognition, plant access to groundwater is often neglected in global evaporation models. This study proposes a new, conceptual approach to incorporate plant access to groundwater in existing global evaporation models. To this end, the Global Land Evaporation Amsterdam Model (GLEAM) is used, and the resulting influence of groundwater on global evaporation is assessed. The new GLEAM-Hydro model relies on the linear reservoir assumption for modelling groundwater flow, and introduces a transpiration partitioning approach to estimate groundwater contributions. Model estimates are validated globally against field observations of evaporation, soil moisture, discharge and groundwater level for the time period 2015–2021, and compared to a regional groundwater model. Results indicate only mild improvements in evaporation estimates, as most eddy-covariance stations are located in energy-limited regions or regions with no plant access to groundwater. The temporal dynamics of the simulated evaporation improves across 75% of the stations where groundwater is a relevant water source. The skill of the model for variables such as soil moisture and runoff remains similar to GLEAM v3. Representing groundwater access influences evaporation in 22% of the continental surface, and it increases evaporation globally by 2.5 mm year^{-1} (0.5% of terrestrial evaporation). The proposed approach enables a more realistic process representation of evaporation under water-limited conditions in satellite-data driven models such as GLEAM, and sets the ground to assimilate satellite gravimetry data in the future.

Plain Language Summary

Groundwater can be a crucial source of water for plants: plants that have access to groundwater through their root system are more likely to survive periods of rainfall scarcity. However, many (satellite-based) models neglect this water source and assume plants only depend on the unsaturated-zone soil moisture. This assumption results in underestimated evaporation values during dry conditions, when groundwater may become the main (or even the only) source of water. In this study, we propose a new approach to incorporate groundwater in an existing global, satellite-based evaporation model. The impact of this modification on the model's accuracy and on the resulting evaporation is evaluated. Representing groundwater increases the evaporation globally by 2.5 mm year^{-1} (0.5%) with much higher increases in certain regions.

1 Introduction

Land evaporation couples the energy and water cycles, cooling the surface (K. Trenberth et al., 2009) and supplying 40% of terrestrial precipitation (Oki & Kanae, 2006; K. E. Trenberth et al., 2007; van der Ent et al., 2010). Accurate evaporation estimates are crucial, not only for improved understanding of the water and energy cycles (e.g. Koppa et al., 2021), but also for specific applications, such as irrigation planning, drought prediction, monitoring ecosystem health, and estimating water availability for societies (Fisher et al., 2017; Vicente-Serrano et al., 2010; Konapala et al., 2020). Unfortunately, *in situ* observations of evaporation are often point-based and limited in space and time, making it difficult to obtain accurate estimates over large, heterogeneous regions and long time periods. As a result, evaporation is often calculated based on meteorological and surface data using either dedicated algorithms, or more complex land surface and hydrological models, in which evaporation uncertainties will propagate to both atmospheric and hydrological variables such as temperature and runoff.

During the past two decades, multiple satellite-based evaporation algorithms have been developed. These algorithms enable the estimation of evaporation globally, including poorly gauged regions, and thus facilitate global-scale applications (Kalma et al., 2008; K. Zhang et al., 2016; J. Zhang et al., 2020). Satellite-based evaporation algorithms often aim to close the energy balance (Bastiaanssen et al., 1998; Su, 2002; Mallick et al., 2014), employ empirical methods based on *in situ* observations (Jung et al., 2009), or compute stress indicators to constrain potential evaporation (Miralles et al., 2011; Fisher et al., 2008). Some of these evaporation products also use soil moisture estimates to assess plant water availability for transpiration (e.g. Miralles et al., 2011; Loew et al., 2016). Similarly, many hydrological (e.g. Samaniego et al., 2010; Bieger et al., 2017) and land surface models (e.g. Clark et al., 2015; Blyth et al., 2021) estimate the evaporation as a function of soil moisture. However, these models often assume plants only have access to the water stored in the unsaturated zone which is solely replenished from the surface, i.e., they assume groundwater is not a relevant water source for transpiration. But in many regions of the world plant roots have access to groundwater (e.g. Miguez-Macho & Fan, 2021; Fan, 2015; Evaristo & McDonnell, 2017; Maxwell & Condon, 2016; Kollet & Maxwell, 2008; Taylor et al., 2013). Miguez-Macho and Fan (2021) use inverse modelling and isotope observations to illustrate that 32% of land evaporation in the Mediterranean originates from groundwater during dry months, whereas the globally-averaged contribution is limited to 1%. Barbeta and Peñuelas (2017) use global isotope data to show that groundwater uptakes constitute on average 49% of evaporation in dry seasons and 28% in wet seasons.

Many studies have explored the added value of incorporating groundwater interactions in existing models. One popular avenue has been the coupling of land surface or hydrological models to a groundwater model (e.g. Tian et al., 2012; Sulis et al., 2017; Maxwell & Miller, 2005; Kuffour et al., 2020; de Graaf et al., 2017; Amanambu et al., 2020). These models typically aim to improve the simulation of soil moisture by introducing interactions with groundwater, which then indirectly influences evaporation estimates. While two-way coupling with groundwater models allows for a more accurate representation of the subsurface, the increased data and computational requirements challenge the application at large scales (Condon et al., 2021; Gleeson et al., 2021) such that it is not routinely applied in global models. To overcome this challenge, several studies propose adding a single groundwater layer that interacts with the soil moisture in the unsaturated zone, assuming that lateral groundwater flow is insignificant at the chosen spatio-temporal resolution (e.g. Yeh & Eltahir, 2005; Lam et al., 2011; Niu et al., 2007; Sutanudjaja et al., 2018). Other approaches include the estimation of groundwater-sourced evaporation directly, for example as a function of the soil moisture (Liu & Luo, 2012; Liu et al., 2015) or the fraction of roots accessing groundwater (Orellana et al., 2012; Laio et al., 2009).

Modelling studies that simulate groundwater-surface interactions typically detect higher groundwater uptake by plant roots under dry conditions (Balugani et al., 2017; Maxwell & Condon, 2016; Lam et al., 2011; Miguez-Macho & Fan, 2021). This is also confirmed with a field experiment by Tfwala et al. (2021) who show that under dry conditions, total transpiration decreases while its groundwater contribution increases. Barbeta and Peñuelas (2017) find that the groundwater uptake is independent of the depth to the groundwater table in saturated soils, which is possibly due to the increased water-uptake efficiency of roots (Orellana et al., 2012). This is also concluded by Beyer et al. (2018) who state that *"even if the fraction of roots reaching the water table is small, the efficiency of tap roots can be hundreds of times larger than roots in drier soil and large amounts of water can be transported"*. However, uncertainty regarding the impact of groundwater on evaporation remains large and stems, among others, from the considered root depth that determines whether plants have access to the aquifer, or soil properties that influence the hydraulic conductivity and the corresponding groundwater level (Keune et al., 2016; Fan et al., 2017; Sulis et al., 2019).

In this study, we propose a novel, conceptual approach to incorporate plant access to groundwater in large-scale models, that is globally applicable owing to limited additional data and computational requirements. The proposed approach is based on two concepts: (i) a linear reservoir for the groundwater flow (e.g. Sutanudjaja et al., 2018; Fenicia et al., 2006; Gao et al., 2014), and (ii) a partitioning of transpiration into contributions from the unsaturated zone and groundwater that reflects an increased groundwater uptake during dry conditions (Liu & Luo, 2012; Liu et al., 2015). The approach is incorporated in the satellite-based Global Land Evaporation Amsterdam Model (GLEAM), and its impact on land evaporation estimates is evaluated. The structure of the paper is as follows: Section 2 describes the new GLEAM-Hydro model. Sections 3 and 4 describe the input data and validation strategy. Results are presented and discussed in Sections 5 and 6, respectively, before conclusions are drawn in Section 7.

2 Methods

This study introduces groundwater-sourced evaporation via plant access to groundwater in GLEAM, creating a new version of the model, hereafter referred to as GLEAM-Hydro. The original GLEAM v3, which does not consider groundwater–vegetation interactions, is used as reference. GLEAM-Hydro is validated regionally over the Netherlands, where a reliable groundwater model and abundant *in situ* groundwater level observations are available, and globally using *in situ* observations of evaporation, soil moisture, discharge and groundwater levels. After validation, the effect of representing plant access to groundwater on global evaporation is assessed by comparing GLEAM-Hydro to the baseline GLEAM v3.

2.1 GLEAM-Hydro

2.1.1 Baseline GLEAM v3

The baseline model for GLEAM-Hydro is GLEAM (Miralles et al., 2011) on its current version 3 (v3) (Martens et al., 2017). GLEAM v3 estimates the total evaporation as the sum of interception loss, transpiration, bare soil evaporation, open-water evaporation, and sublimation. Transpiration (E_{t}) is estimated by constraining potential evaporation (E_{p}) with a stress factor S_{t} (i.e., $E_{\mathrm{t}} = S_{\mathrm{t}} \cdot E_{\mathrm{p}}$) which is a function of soil moisture and vegetation optical depth (VOD) to account for changes in phenology. Similarly, bare soil evaporation (E_{b}) is estimated using a stress factor which is a function of the soil moisture only (Martens et al., 2017). Potential evaporation is estimated with the Priestley and Taylor (1972) equation. Within each grid cell, the following four land cover types are distinguished: tall vegetation, short vegetation, bare soil, and open water bodies. The root zone is divided into three soil layers (0–0.1 m, 0.1–1 m, 1–2.5 m) depending on the land cover fraction, i.e., tall vegetation has three soil layers, short vegetation two, and bare soil a single layer. Below the bottom soil layer, the water content is assumed to be at field capacity at all times, and a free drainage approach is applied. Thus, in GLEAM v3 E_{t} and E_{b} depend only on the energy demand (i.e., E_{p}) and water availability in each soil layer (i.e., w) — see Martens et al. (2017) for more information.

2.1.2 Groundwater reservoir: water balance

In GLEAM-Hydro, the groundwater system is represented by a single reservoir with only one inflow (i.e., recharge) and multiple fluxes leaving the system (i.e., baseflow, evaporation and overland flow), assuming lateral groundwater flows are insignificant. The groundwater reservoir is implemented at the grid cell level, i.e., the groundwater level is assumed to be the same for all land cover classes, and comprises the entire soil column. The implementation further allows to differentiate between the water volumes stored in the saturated zone in and/or below the three soil layers (S_{s}), and the groundwater levels (GWL).

The water balance for S_{s} is estimated with

$$\frac{dS_{\mathrm{s}}}{dt} = Q_{\mathrm{r}} - Q_{\mathrm{s}} - E_{\mathrm{GW}} - Q_{\mathrm{OF}} \tag{1}$$

with Q_r recharge into saturated zone [mm d^{-1}], Q_s groundwater flow [mm d^{-1}], E_GW groundwater-sourced evaporation [mm d^{-1}], and Q_OF overland flow [mm d^{-1}]. The groundwater level GWL is then estimated using the specific yield (θ_y) to obtain absolute levels rather than water volumes (Lv et al., 2021; Healy & Cook, 2002):

$$GWL = \frac{1}{\theta_\mathrm{y}} \cdot S_\mathrm{s} \tag{2}$$

$$\theta_\mathrm{y} = \theta_\mathrm{por} - \theta_\mathrm{flc} \tag{3}$$

with θ_y specific yield [m^3 m^{-3}], θ_por soil porosity [m^3 m^{-3}], and θ_flc field capacity [m^3 m^{-3}].

2.1.3 Groundwater fluxes: Recharge, baseflow and overland flow

The recharge is assumed to be equal to the drainage leaving the bottom soil layer across all land cover classes. The groundwater flow is estimated with the linear reservoir assumption, as commonly used in (global) hydrological models (e.g. Sutanudjaja et al., 2018; Gao et al., 2014; Samaniego et al., 2010):

$$Q_\mathrm{s} = \max(0, S_\mathrm{s}) \cdot K_\mathrm{s} \tag{4}$$

with the recession constant K_s [d^{-1}]. When plant roots have access to groundwater, groundwater-sourced evaporation is greater than zero and estimated with Eq. 6 and 9 (see Section 2.1.4). Overland flow occurs when groundwater levels exceed the surface level:

$$Q_\mathrm{OF} = \frac{\max(0, GWL \cdot \theta_\mathrm{y})}{\Delta t} \tag{5}$$

with Δt is the time step which is equal to one day [d]. Note that the land surface is used as reference for the groundwater level, which is defined as negative below the surface and positive above the surface.

2.1.4 Groundwater fluxes: Groundwater-sourced evaporation

When plants do not have access to groundwater, then all the water stored in the root zone comes from the surface through infiltration (see Fig. 1a). However, when plants have access to groundwater, then water for evaporation originates from both infiltration ($E_\mathrm{t,nonGW}$) and groundwater ($E_\mathrm{t,GW}$, see Fig. 1b). We assume that plants extract water first from the groundwater system, assuming water is more easily accessible there, after which plants extract water from soil moisture stored above the water table. Note that the maximum rooting depths considered here are 0.1–2.5 m depending on the land cover class (see Section 2.1.1), and that plants cannot access the groundwater system beyond that depth in GLEAM-Hydro.

To distinguish between the uptake of groundwater and infiltrated water for transpiration, the groundwater contribution fraction (f_GW, [-]) is introduced as:

$$f_\mathrm{GW} = \min(1, \max(0, \frac{1}{l_\mathrm{sat,max}} \cdot \sum_{l=1}^{l_\mathrm{sat,max}} \frac{\theta_\mathrm{l,flc} - w_\mathrm{l}}{\theta_\mathrm{l,flc} - \theta_\mathrm{l,crt}})) \tag{6}$$

with l soil layer number [-], $l_\mathrm{sat,max}$ maximum number of soil layers in the root zone affected by groundwater [-], θ_flc field capacity [m^3 m^{-3}], w soil moisture [m^3 m^{-3}], and θ_crt critical soil moisture [m^3 m^{-3}]. The relative contribution of groundwater to transpiration is defined such that it is highest under dry conditions and lowest under wet conditions; i.e., $f_\mathrm{GW} = 1$ if $w \leq \theta_\mathrm{crit}$ (dry soil) and $f_\mathrm{GW} = 0$ if $w \geq \theta_\mathrm{flc}$ (wet soil). If the groundwater affects multiple soil layers, then the fraction is averaged over the affected layers.

Transpiration is divided into $E_\mathrm{t,GW}$ and $E_\mathrm{t,nonGW}$ by incorporating f_GW into the evaporative stress factor:

$$S_\mathrm{t} = f_\mathrm{GW} \cdot S_\mathrm{t,GW} + (1 - f_\mathrm{GW}) \cdot S_\mathrm{t,nonGW} \tag{7}$$

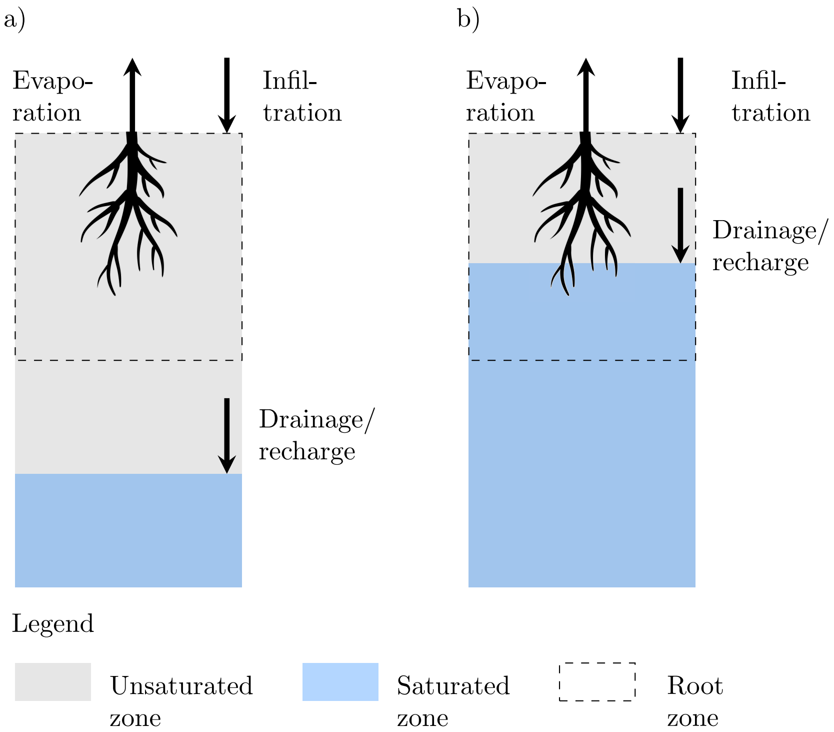

Figure 1. Scheme of plant water sources available for evaporation. a) Deep groundwater: water in the root zone originates only from infiltration (for example rainwater, irrigation, snow melt etc.), b) Shallow groundwater: water in the root zone originates from infiltration and groundwater.

with S_{t} combined stress factor [-], $S_{\mathrm{t,GW}}$ groundwater stress factor [-], and $S_{\mathrm{t,nonGW}}$ non-groundwater stress factor [-]. By definition, $S_{\mathrm{t,GW}} = 1$ since there is no stress in the saturated zone. Analogous to GLEAM v3, $S_{\mathrm{t,nonGW}}$ is a function of soil moisture in the unsaturated zone (Martens et al., 2017).

Transpiration E_{t} [mm d^{-1}] is then calculated as

$$E_{\mathrm{t}} = f_{\mathrm{GW}} \cdot S_{\mathrm{t,GW}} \cdot E_{\mathrm{p}} + (1 - f_{\mathrm{GW}}) \cdot S_{\mathrm{t,nonGW}} \cdot E_{\mathrm{p}} \tag{8}$$

with

$$E_{\mathrm{t,GW}} = f_{\mathrm{GW}} \cdot S_{\mathrm{t,GW}} \cdot E_{\mathrm{p}} \tag{9}$$

the transpiration that is sourced from groundwater [mm d^{-1}], and

$$E_{\mathrm{t,nonGW}} = (1 - f_{\mathrm{GW}}) \cdot S_{\mathrm{t,nonGW}} \cdot E_{\mathrm{p}} \tag{10}$$

the transpiration sourced from soil moisture in the unsaturated zone [mm d^{-1}].

This approach is applied for all land cover fractions individually, i.e., for tall vegetation, short vegetation and bare soil. The latter is included to represent water evaporating from shallow groundwater directly without root extraction (Balugani et al., 2017). The aggregated groundwater-sourced evaporation (E_{GW}) is then used in the water balance equation (Eq. 1).

With this approach, the total stress factor S_{t} cannot exceed 1, meaning that the total transpiration is always equal to or below potential evaporation. In addition, we assume that there is unlimited groundwater available for E_{GW}, hence it does not depend on S_{s}. As a result, E_{GW} can potentially surpass the water volume stored in the groundwater reservoir, resulting in negative S_{s} values and groundwater levels lower than the initial condition (see Section 2.2). In that case, there is no groundwater flow until the reservoir is refilled and S_{s} values are positive again (see Eq. 4). Furthermore, the two water sources available for evaporation in the root zone (infiltrated water and groundwater) are treated separately for simplicity. In other words, groundwater does not directly influence the unsaturated-zone soil moisture reservoir, i.e., that reservoir is not saturated at or below the groundwater level, which allows retaining the original drainage function in GLEAM. Nevertheless, this approach indirectly mimics the interaction between the unsaturated and saturated zone: With shallow groundwater levels, the water content in the unsaturated zone becomes comparatively higher, as plants partly extract water from the groundwater instead of extracting only from the unsaturated zone.

2.2 Experiments set-up

GLEAM v3 and GLEAM-Hydro are run on daily timescale at 0.25° resolution and for the time period 2015–2021. Global analyses cover all land regions within 90°N–90°S and 180°E–180°W, whereas analyses for the Netherlands cover the region 3°E–7.5°E and 50.5°N–54°N. In GLEAM-Hydro, initial conditions for GWL are based on the global water table depth from Fan et al. (2013) using the monthly mean values for January. Initial conditions for S_{s} are obtained through a spin-up, in which the model is run over the full period (2015–2021). The spin-up starts with long-term mean values for S_{s} which is estimated with the water balance equation (Eq. 1) assuming $\frac{d\bar{S}_{\mathrm{s}}}{dt} \approx 0$, zero groundwater-sourced evaporation and overland flow, applying Eq. 4 for Q_{s}, and using recharge (Q_{r}) from GLEAM v3. Initial conditions for S_{s} to run GLEAM-Hydro are then based on the median S_{s} in January from the spin-up period.

3 Input data

Satellite observations and reanalysis datasets are used as input. Air temperature is obtained from Atmospheric Infrared Sounder (AIRS) level 3 version 7.0 (Aumann et al., 2003). Net radiation and shortwave outgoing radiation are obtained from Clouds and the Earth's Radiant Energy System (CERES) Edition 4.1 (Wielicki et al., 1996). Precipitation data are obtained from the Multi-Source Weighted-Ensemble Precipitation (MSWEP) version 2.8 (Beck et al., 2019). Snow water equivalent is based on GLOBSNOW v2.0 observations (Takala et al., 2011). Vegetation optical depth (VOD) is based on the Vegetation Optical Depth Climate Archive (VODCA, Moesinger et al., 2020). Finally, land cover class fractions are derived from MOD44B version 6 Vegetation Continuous Fields (VCF, DiMiceli et al., 2015). All observations are available globally and, if needed, interpolated bi-linearly to 0.25° resolution. These observations are used in both GLEAM v3 and GLEAM-Hydro consistently. In addition, GLEAM-Hydro includes recession constant data which are derived globally by Sutanudjaja et al. (2018) for the PCRaster GLOBal Water Balance model (PCR-GLOBWB). Furthermore, global water table depth observations according to Fan et al. (2013) are employed for the initial conditions as mentioned in Section 2.2.

4 Validation

4.1 *In situ* observations

Global *in situ* observations with respect to evaporation, soil moisture, discharge and groundwater level are collected for the study period 2015–2021 from 10,951 sites. These observations are obtained from multiple platforms including AmeriFLUX, European Fluxes Database Cluster (EFDC), FLUXNET-CH4, Global Runoff Data Centre (GRDC), Integrated Carbon Observation System (ICOS), International Groundwater Resources Assessment Centre (IGRAC), and International Soil Moisture Network (ISMN). See Table A1 for more information regarding observation type, number of sites per source, website links and references. These observations include not only variables directly used for validation, but also additional variables used, for example, to filter rain and snow days (i.e., precipitation, air temperature, snow depth, net radiation, surface heat flux and ground heat flux) — see below. For the Netherlands, the above-mentioned global databases provide data to validate evaporation and soil moisture. In addition, groundwater level observations at 2750 sites are available from the DINO (*Data en Informatie van de Nederlandse Ondergrond*) database.

In situ observations are pre-processed to remove outliers (values smaller or larger than the 1^{st} or 99^{th} percentile, respectively), duplicates, and daily observations with low quality flag or coverage (<25%) at sub-daily scale where available. When validating evaporation, rain days (> 0 mm d^{-1}) and stations with a poor energy balance closure are removed ($\frac{R_\mathrm{n}-G-H}{LE} > 0.2$ with R_n net radiation, G ground heat flux, H surface heat flux, and LE latent heat flux). Evaporation is calculated from latent heat flux observations using air temperature data. When validating with respect to soil moisture, days with snowfall (> 10 mm) or low temperature ($< 0°$C) are removed. GLEAM-based soil moisture estimates are linearly interpolated to the depth of the observation. Sites with less than 365 observation points within the study period are removed. In case of gaps in the *in situ* observations used for the filtering procedure — i.e., gaps in precipitation, snow or temperature data at the station — GLEAM forcing data are used too. For the validation of runoff, stations with a temporal coverage of less than 75% are removed. In addition, discharge stations are removed when the corresponding gridded basin area at 0.25°resolution deviates substantially from the actual area as provided by GRDC (i.e., $|\frac{A_\mathrm{gridded}-A_\mathrm{actual}}{A_\mathrm{actual}}| > 0.2$). Also, stations with a basin area smaller than 2500 km^2 are not considered. Further, nested river basins are avoided by favouring downstream stations. Similar approaches for *in situ* data pre-processing have been applied in previous studies (Martens et al., 2020, 2017). Appendix Fig. A1 visualises all the stations available for validation after pre-processing.

4.2 Regional validation: The Netherlands

Regional simulations of GLEAM v3 and GLEAM-Hydro for the Netherlands are validated using *in situ* data from 4 eddy-covariance, 22 soil moisture and 1714 groundwater level sites. See Section 4.1 for more information on the *in situ* observations used.

To assess the accuracy of the groundwater level estimates of GLEAM-Hydro, groundwater levels from the groundwater model LHM version 4.1 (*Landelijk Hydrologisch Model*, `https://www.nhi.nu/nl/index.php/modellen/lhm/`) are used as a reference. LHM v4.1 uses MODFLOW (Langevin et al., 2017) for the saturated zone, and other models for the remaining components such as the unsaturated zone, surface water and routing (Janssen et al., 2020). Note that this model does not consider feedbacks of evaporation on groundwater levels. LHM-based groundwater level estimates are also validated against the same 1714 groundwater level sites. As LHM simulations are only available until 2018, groundwater level validations over the Netherlands are done for the time period 2015–2018. The remaining variables are validated over the entire study period (2015–2021), depending on *in situ* data availability.

4.3 Global validation

Global simulations of GLEAM v3 and GLEAM-Hydro are validated for the time period 2015–2021 using 100 eddy-covariance, 3422 soil moisture, 97 discharge and 1329 groundwater level sites (Fig. A1 in the Appendix). See Section 4.1 for more information on the *in situ* observations used.

4.4 Performance metrics

Evaporation, soil moisture and groundwater levels are validated by comparing observations and simulated time series from the respective grid cells where the stations are located. For this purpose, the following performance metrics are used: Spearman correlation coefficient (R), root mean square error ($RMSE$), and Kling-Gupta efficiency (KGE, Gupta et al., 2009). R ranges between -1 and 1, $RMSE$ between 0 and ∞, and KGE between $-\infty$ and 1. A "perfect" performance is represented by $R = 1$, $RMSE = 0$ and $KGE = 1$. If the reference level of groundwater observations is unknown, performance metrics are estimated using groundwater level anomalies, i.e., the observed and estimated data are subtracted by their mean using identical observation days.

Runoff from GLEAM is estimated based on the long-term water balance, assuming storage changes are insignificant compared to the magnitude of the fluxes over the simulation period, i.e., $\bar{Q} = \bar{P} - \bar{E}$. Runoff estimates are compared to discharge observations and their accuracy is evaluated with the mean difference ($MD = \bar{Q}_{\mathrm{GLEAM}} - \bar{Q}_{\mathrm{In\ situ}}$) and the percentage bias ($PBIAS = \frac{|\bar{Q}_{\mathrm{GLEAM}} - \bar{Q}_{\mathrm{In\ situ}}|}{\bar{Q}_{\mathrm{In\ situ}}} \cdot 100\%$).

5 Results

5.1 GLEAM-Hydro validation

5.1.1 Regional validation: The Netherlands

Evaporation

In the Netherlands and the near surroundings, evaporation is represented well by the reference model, GLEAM v3, with a median correlation of $R_{\mathrm{median}} = 0.90$. The other performance metrics agree with the skill indicated by the correlation, with $RMSE_{\mathrm{median}} = 0.85$ mm d^{-1} and $KGE_{\mathrm{median}} = 0.78$ for GLEAM v3. Incorporating plant access to groundwater with GLEAM-Hydro does not affect these performance metrics and retains the median accuracy of the simulations (Table 1 and Fig. 2). However, this assessment is based on only 4 eddy-covariance stations of which only 1 station (at Cabauw, 51.97°N and 4.93°E) is located in a region with shallow groundwater levels (above -2.5 m). In addition, this station is located in a region that is primarily energy-limited, as any other station in the Netherlands. During the simulation period, 94% of the days at Cabauw show no or only little water limitation, i.e., $E_{\mathrm{p}} - E < 0.5$ mm d^{-1}, which results in a small evaporation increase from 617.2 mm year^{-1} (GLEAM v3) to 630.4 mm year^{-1} (GLEAM-Hydro). Hence, over the Netherlands, groundwater barely affects the magnitude of transpiration.

Soil moisture

The soil moisture is represented reasonably well by the reference model GLEAM v3 with a median correlation of $R_{\mathrm{median}} = 0.74$. The remaining performance metrics are $RMSE_{\mathrm{median}} = 7.69\%$ and $KGE_{\mathrm{median}} = 0.49$ for GLEAM v3 (Table 1). Incorporating plant access to groundwater with GLEAM-Hydro does not affect the skill of the simulated soil moisture over the Netherlands (Table 1 and Fig. 2c). This assessment is based on 22 sites, yet only 1 site is located in a region with shallow groundwater levels (in Bergambacht near Cabauw, 51.93°N and 4.79°E). Also this station is located in an energy-limited region where 94% of the days show no water limitation and where the impact of groundwater on evaporation is small.

Groundwater level

The groundwater level dynamics over the Netherlands are represented well by GLEAM-Hydro with a median correlation of $R_{\mathrm{median}} = 0.78$ (Table 1). The median correlation is only slightly better with LHM, despite the latter being calibrated for the Netherlands (Table 1 and Fig. 2d). In both models, correlations are greater than 0.5 at 88% of the sites, with a standard deviation (σ) in the correlations of $R_{\sigma} = 0.21$. LHM shows slightly better median $RMSE$ and KGE values than GLEAM-Hydro (Table 1). Based on the correlation

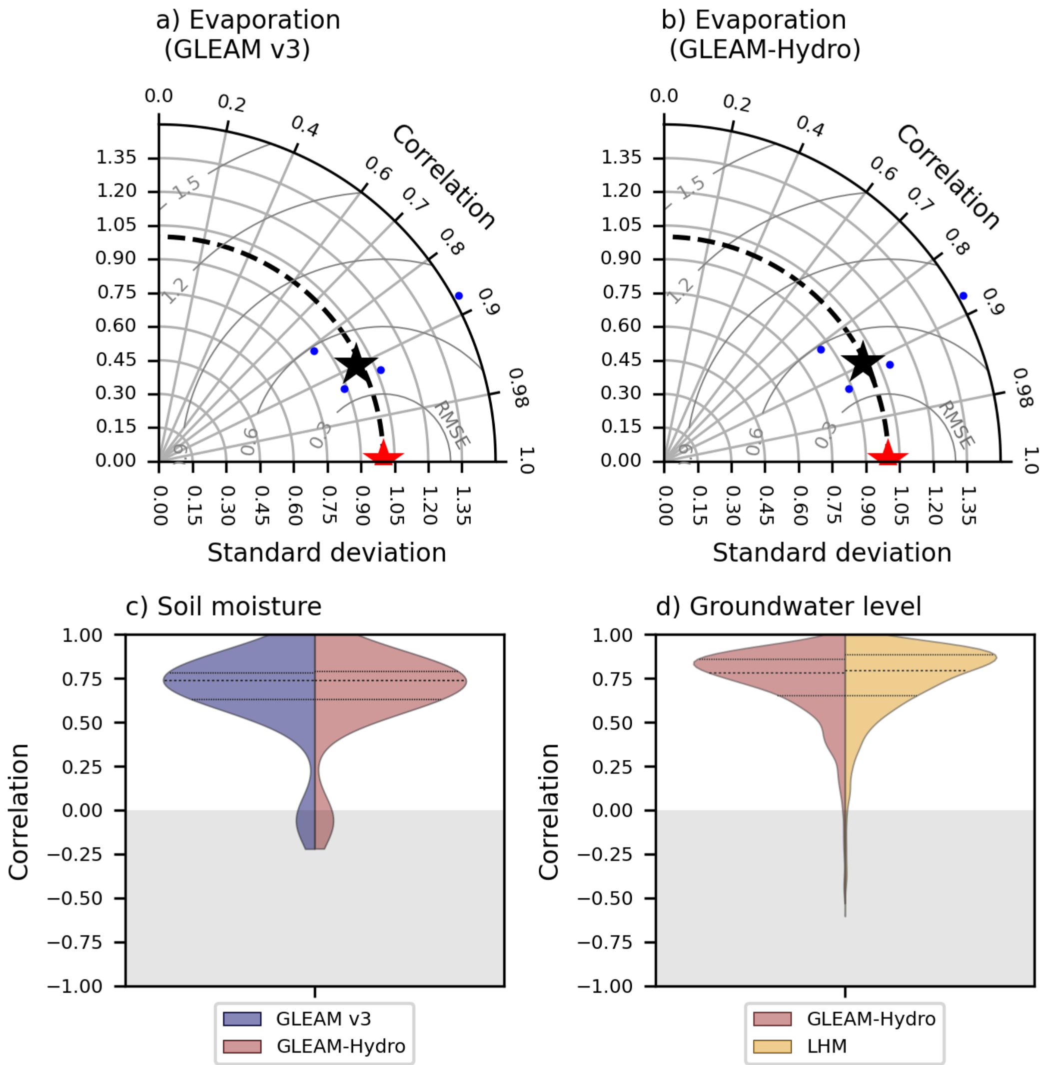

Figure 2. a)–b) Taylor diagrams illustrating the performance of (a) GLEAM v3 and (b) GLEAM-Hydro with respect to evaporation for the Netherlands. The standard deviation and RMSE are normalised using the standard deviation of the observed time series such that the red star serves as reference point. c)–d) Violin plots illustrating the validation of (c) soil moisture and (d) groundwater level based on the correlation.

coefficients, 44% of the sites perform better or similarly well with GLEAM-Hydro compared to LHM (62% based on $RMSE$, 34% based on KGE). Fig. 3a shows an example of a station where groundwater levels are estimated better with GLEAM-Hydro than LHM (GLEAM-Hydro: $R = 0.64$, $RMSE = 0.05$ m, $KGE = 0.62$, LHM: $R = 0.22$, $RMSE = 1.37$ m, $KGE =$ -1.36), whereas Fig. 3b illustrates the opposite (GLEAM-Hydro: $R = 0.85$, $RMSE = 0.67$ m, $KGE = 0.45$, LHM: $R = 0.92$, $RMSE = 0.12$ m, $KGE = 0.80$).

At multiple sites, significant biases are detected in the simulated groundwater level (see Fig. A2 in the Appendix). The groundwater level bias in GLEAM-Hydro is a result of the bias in the initial conditions. In GLEAM-Hydro (LHM), $RMSE$ is smaller than 5 m at 97% (96%) of the sites.

Table 1. Median statistics for the Netherlands for different variables and GLEAM versions. Performance metrics include correlation (R), root mean square error ($RMSE$), and Kling-Gupta Efficiency (KGE).

Median values		GLEAM v3	GLEAM-Hydro	LHM	Unit
Evaporation	R	0.90	0.90	n/a	-
	RMSE	0.85	0.85	n/a	mm d^{-1}
	KGE	0.78	0.79	n/a	-
Soil moisture	R	0.74	0.74	n/a	-
	RMSE	7.69	7.94	n/a	%
	KGE	0.49	0.49	n/a	-
Groundwater	R	n/a	0.78	0.79	-
	RMSE	n/a	0.98	0.73	m
	KGE	n/a	-0.18	0.02	-

Overall, the groundwater representation in GLEAM-Hydro is able to mimic the skill of LHM in simulating groundwater levels. The degree of uncertainty, i.e., the variation in the performance metrics, in GLEAM-Hydro is comparable to LHM (Fig. 2d).

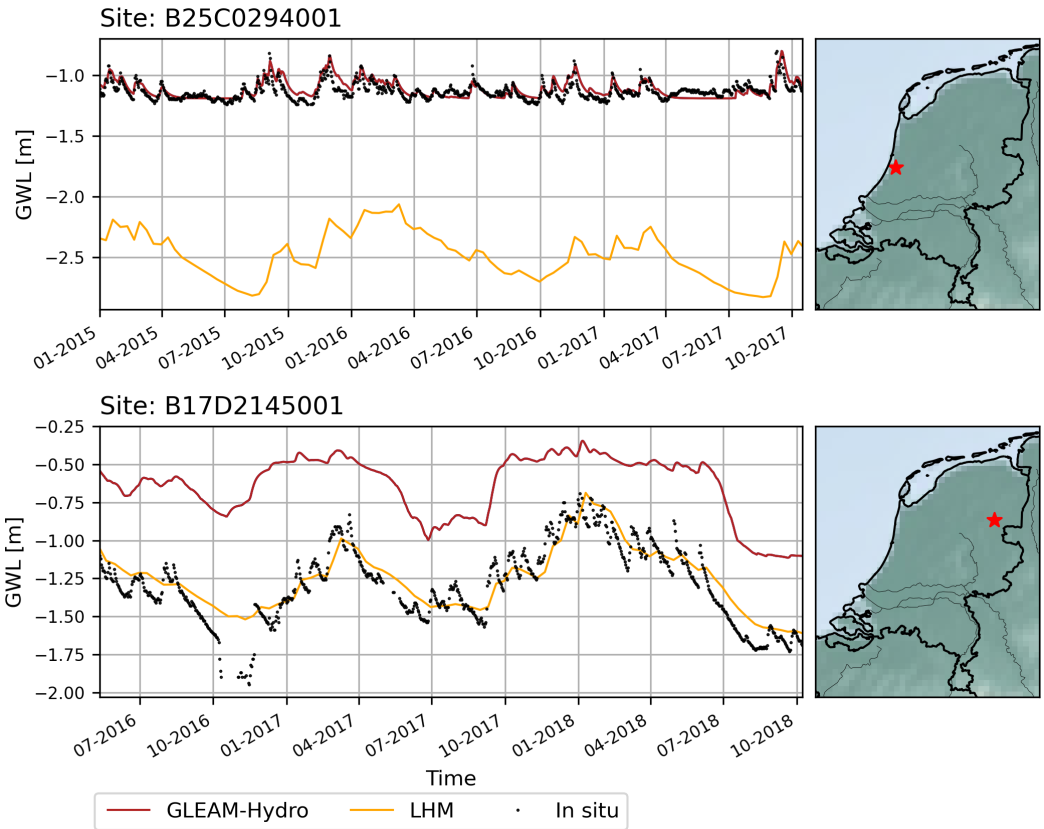

Figure 3. Time series of groundwater levels at two sample locations in the Netherlands, comparing GLEAM-Hydro and LHM with observations from corresponding well observations. The sites are located in (a) the province North-Holland (52.33°N and 4.64°E), and (b) the province Drenthe (52.72°N and 6.53°E).

5.1.2 Global validation

Evaporation

Across all eddy-covariance stations available globally, evaporation from GLEAM v3 is already represented well with a median correlation of $R_{\text{median}} = 0.81$, which is similar to previous studies (Martens et al., 2017). The remaining performance metrics amount to $RMSE_{\text{median}} = 1.01$ mm d^{-1} and $KGE_{\text{median}} = 0.49$ for GLEAM v3 (Table 2). Incorporating groundwater in GLEAM-Hydro does not influence the median performances significantly (see Fig. 4 and Table 2) as, again, many stations are located in regions with energy-limited conditions or deep groundwater levels (see Fig. A1a in the Appendix). Note that in only 39% of the continental surface, average groundwater levels simulated by GLEAM-Hydro are shallower than -2.5 m. When considering only stations where groundwater becomes a relevant water source for transpiration (8 out of 100 stations), then the median correlation improves from $R_{\text{GLEAMv3}} = 0.66$ to $R_{\text{GLEAM-Hydro}} = 0.69$ (Fig. 4c and Table 2), indicating the temporal dynamics of evaporation are better simulated if groundwater is considered as a source for transpiration. However, this improvement is not reflected in the median KGE and $RMSE$ values (see Table 2), as only 4 of the 8 stations improved with respect to $RMSE$ and KGE. See Fig. 5 for an example eddy-covariance station in Italy, where the incorporation of groundwater in the model influences evaporation and increases the accuracy of the estimates. There, the maximum evaporation increase due to groundwater access is 2.5 mm d^{-1}. The correlation increases from $R = 0.82$ in GLEAM v3 to $R = 0.89$ in GLEAM-Hydro, and the $RMSE$ and KGE change from $RMSE = 0.82$ mm d^{-1} and $KGE = 0.82$ (GLEAM v3) to $RMSE = 0.89$ mm d^{-1} and $KGE = 0.68$ (GLEAM-Hydro).

Table 2. Median statistics for different variables and GLEAM versions with respect to all stations globally, and in brackets with respect to stations where groundwater is a relevant water source. Performance metrics include correlation (R), root mean square error ($RMSE$), and Kling-Gupta Efficiency (KGE).

Median values		GLEAM v3	GLEAM-Hydro	Unit
Evaporation	R	0.81 (0.66)	0.81 (0.69)	-
	RMSE	1.01 (1.20)	1.02 (1.32)	mm d^{-1}
	KGE	0.49 (0.32)	0.48 (0.19)	-
Soil moisture	R	0.71 (0.67)	0.71 (0.63)	-
	RMSE	9.49 (9.44)	9.51 (9.13)	%
	KGE	0.26 (0.30)	0.26 (0.26)	-
Groundwater	R	n/a	0.22 (-0.03)	-
	RMSE	n/a	1.60 (0.75)	m
	KGE	n/a	-0.87 (-0.86)	-

Soil moisture

The soil moisture from GLEAM v3 is represented well at most sites with $R_{\text{median}} = 0.71$ (Table 2), which is similar to previous studies (Martens et al., 2017; Beck et al., 2021). The remaining performance metrics amount to $RMSE_{\text{median}} = 9.49\%$ and $KGE_{\text{median}} = 0.26$. Similar to evaporation, the soil moisture performance does not change substantially when incorporating plant access to groundwater (see Fig. 4d and Table 2). The differences remain small also when validating only for sites where groundwater becomes a relevant water source for transpiration (Table 2), which is the case for 143 out of 3422 sites (see Fig. A1b in the Appendix). At those sites, the performance metrics change slightly, without clear signals for improvement, from $R = 0.67$, $RMSE = 9.44\%$ and $KGE = 0.30$ for GLEAM v3 to $R = 0.63$, $RMSE = 9.13\%$ and $KGE = 0.26$ for GLEAM-Hydro (Table 2). Note, that changes in the soil moisture only occur indirectly through altered transpiration (see Section 2.1.4).

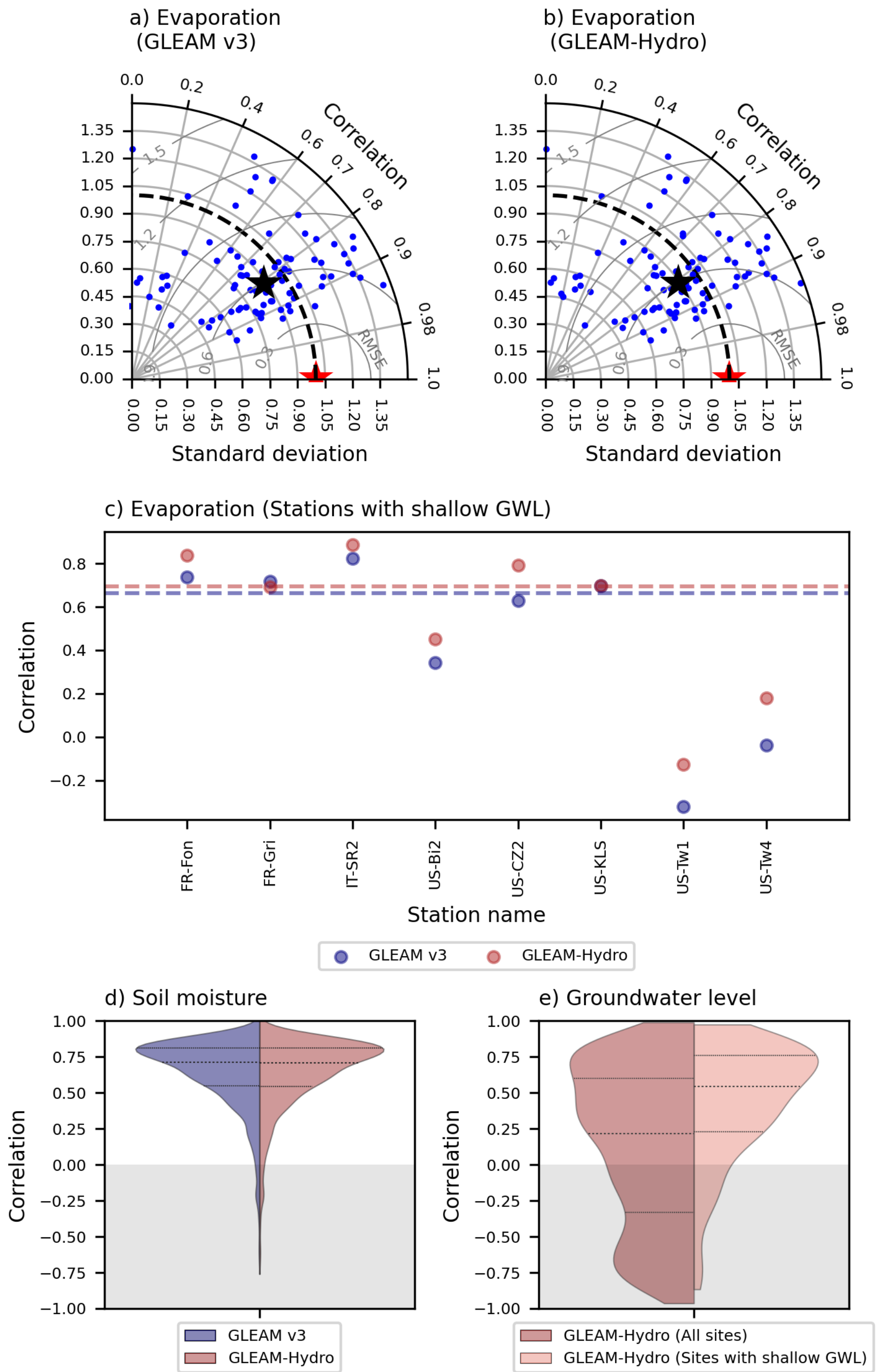

Figure 4. a)–b) Taylor diagrams illustrating the global performance of (a) GLEAM v3 and (b) GLEAM-Hydro with respect to evaporation. The standard deviation and RMSE are normalised using the standard deviation of the observed time series such that the red star serves as reference point. c) Correlation of evaporation simulated with GLEAM v3 (blue) and GLEAM-Hydro (red) against observations at those eddy-covariance stations that are influenced by groundwater. The dashed line indicates the median correlation over the selected stations. d)–e) Violin plots illustrating the validation of (d) soil moisture and (e) groundwater level based on the correlation.

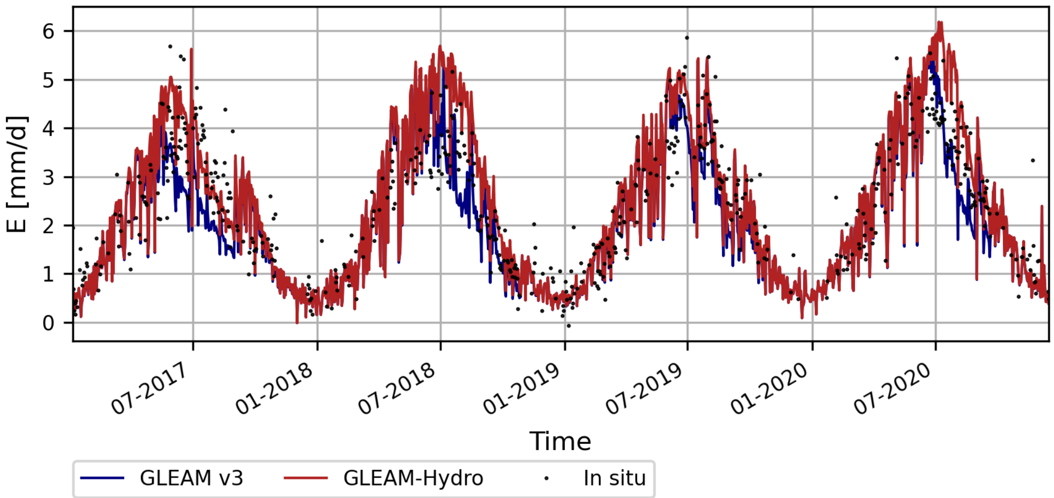

Figure 5. Evaporation at the eddy-covariance tower San Rossore 2 in Italy (IT-SR2 at 43.73°N and 10.29°E) and as simulated with GLEAM v3 and GLEAM-Hydro.

Runoff

Over all stations, the average runoff over the simulation period is represented reasonably well with GLEAM v3 compared to the discharge observations, with $R = 0.84$ (Fig. A3a in the Appendix). The median MD is equal to MD_{median} = -123.2 mm year^{-1} (Fig. A3b in the Appendix), largely reflecting biases in precipitation and/or the simulated evaporation. The median percent bias amounts to $PBIAS_{\text{median}}$ = 40.4%. Overall, runoff is overestimated at 11 of the 97 stations with GLEAM v3, and underestimated at 81 stations. Runoff is simulated well at 5 stations, where only small biases (i.e., $|MD| < 10$ mm year^{-1}) are found.

Incorporating plant access to groundwater in GLEAM-Hydro leads to a slight correlation increase ($R = 0.85$), and the MD changes between ΔMD = 0.0–30.7 mm year^{-1} with $\Delta MD = MD_{\text{GLEAM v3}} - MD_{\text{GLEAM-Hydro}}$. Changes in the percent bias range between $\Delta PBIAS$ = -105.6–40.6% ($\Delta PBIAS = PBIAS_{\text{GLEAM v3}} - PBIAS_{\text{GLEAM-Hydro}}$) with positive values indicating runoff improved with GLEAM-Hydro (Fig. A3c and d in the Appendix). At 61 of the 97 stations, runoff changes are small ($\Delta|PBIAS| < 1\%$) as groundwater access is limited in the basins associated with these stations.

Compared to GLEAM v3, evaporation in GLEAM-Hydro either increases when groundwater is a relevant source for transpiration, or remains the same when the groundwater level is too deep. Hence, the long-term averaged runoff can only decrease or remain the same. Therefore, the skill of those stations that overestimate runoff with GLEAM v3 (11 of 97 stations) improve (8 stations) or remain the same (3 stations). On the other hand, at those stations that already underestimate runoff with GLEAM v3 (81 of 97 stations), the bias further increases with GLEAM-Hydro, except when the roots have no access to the groundwater level. This results in a decreased accuracy at 24 of the 81 stations that already underestimate runoff with GLEAM v3.

Groundwater level

The global groundwater level performance varies considerably among the 1329 sites (Fig. 4e). The median correlation of simulated groundwater levels in GLEAM-Hydro with observations is equal to $R_{\text{median}} = 0.22$. This increases to $R_{\text{median}} = 0.54$ when considering only those sites with shallow water table depths, i.e., where plants have access to the groundwater system based on the modelled or observed groundwater levels. The remaining performance metrics amount to $RMSE_{\mathrm{median}}$ = 1.60 m and KGE_{median} = -0.87 when considering all sites (Table 2). The correlation is greater than 0.5 at 31% of the sites (Fig. A4 in the Appendix) and $RMSE$ is smaller than 5 m at 62% of the sites (Fig. A5 in the Appendix). As an example, Fig. A6 in the Appendix shows the time series of observed and simulated groundwater level for a well represented station near Philadelphia in the United States (at 74.84°W and 39.99°N, $R = 0.85$, $RMSE = 0.21$ m, $KGE = 0.83$).

5.2 Global influence of groundwater on evaporation

Representing plant access to groundwater increases the annual-mean, globally-averaged terrestrial evaporation from 392.4 mm year^{-1} to 394.8 mm year^{-1}. This corresponds to an increase of 2.5 mm year^{-1} globally-averaged; the standard deviation of all land pixels amounts to 11.0 mm year^{-1}. In other words, the terrestrial evaporation increases with 404 km^3 year^{-1} over the continental surface, from 74,064 km^3 year^{-1} (GLEAM v3) to 74,468 km^3 year^{-1} (GLEAM-Hydro). Relative to GLEAM v3, the annual-mean, globally-averaged evaporation increases with 0.5% with a standard deviation of 2.2%. The globally-averaged groundwater contribution to evaporation f_{GW} is equal to 0.008 with a standard deviation of 0.03.

The maximum local increase of annual-mean evaporation is 245.2 mm year^{-1} (Fig. 6) or 149.7% relative to GLEAM v3 (Fig. A7 in the Appendix). The aggregated mean groundwater contribution to evaporation f_{GW} reaches up to 0.36. At daily-scale, the evaporation increases locally up to 5.5 mm d^{-1}. Large evaporation increases are observed in for example Canada, Russia, and several regions in Congo and South America. In those regions, the groundwater level is shallow (Fan et al., 2013) as illustrated in Fig. A8 in the Appendix. Hence, groundwater-sourced evaporation is, as expected, strongly influenced by the groundwater level (Fig. 7a–f).

Finally, groundwater-sourced evaporation is the highest in drylands, i.e., in regions with an aridity index larger than 0.65 (Fig. 7). Moreover, groundwater-sourced evaporation is higher for tall vegetation compared to short vegetation and bare soil (Fig. 7h) — which is expected given the deeper roots of tall vegetation (see Section 2.1.1).

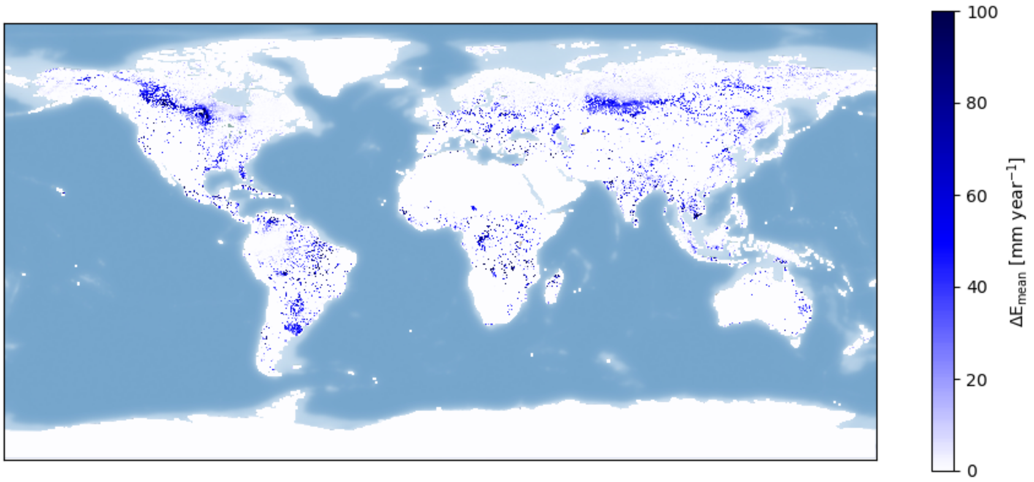

Figure 6. Average evaporation increase due to the incorporation of plant access to groundwater in GLEAM ($\Delta E = E_{\mathrm{GLEAM-Hydro}} - E_{\mathrm{GLEAM\ v3}}$) averaged over the study period.

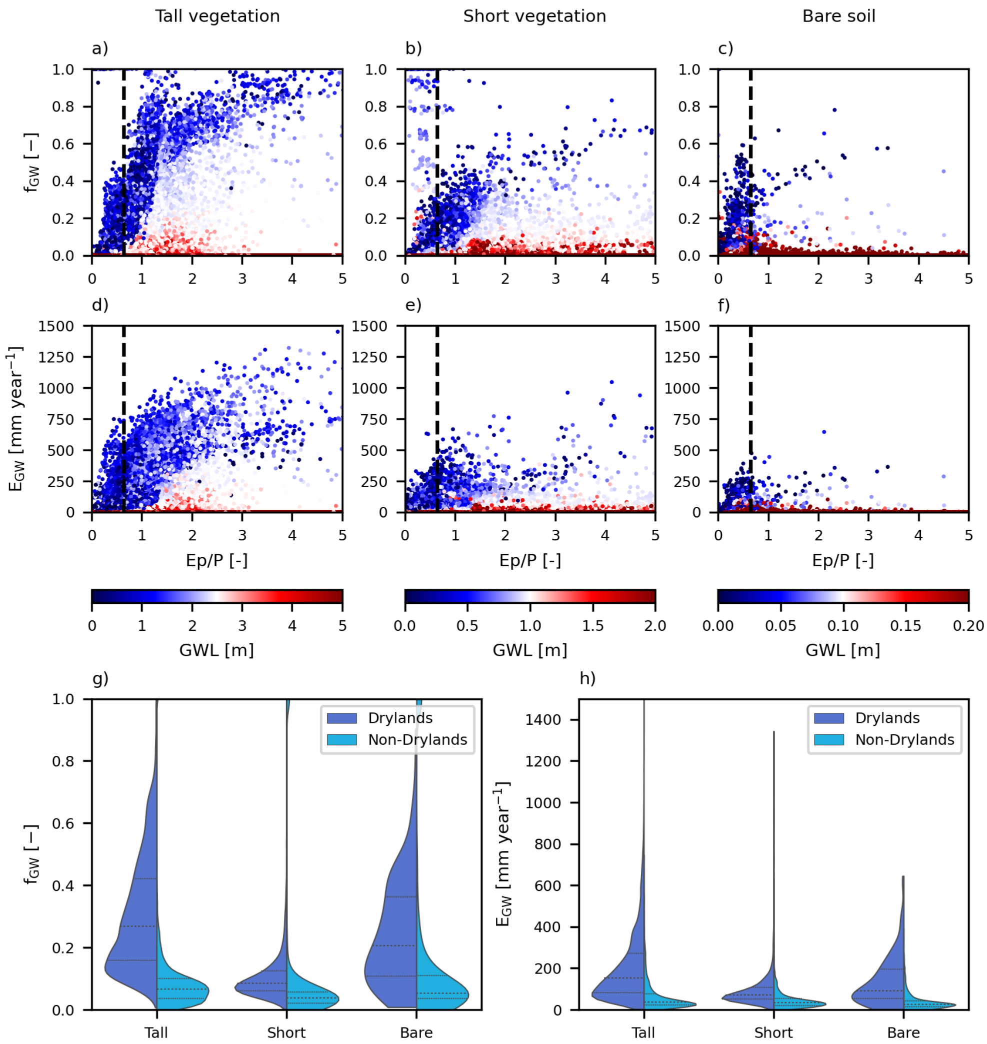

Figure 7. Groundwater contribution fraction (f_{GW}) and groundwater-sourced evaporation (E_{GW}) for tall vegetation, short vegetation and bare soil (a)–(f) as a function of aridity (Ep/P) and groundwater levels (GWL), and (g)–(h) distinguishing between drylands ($E_p/P > 0.65$) and non-drylands ($E_p/P < 0.65$). Results are averaged over the study period.

6 Discussion

This study has introduced groundwater-sourced evaporation in the satellite-based evaporation model GLEAM. A novel, conceptual approach of groundwater–vegetation interactions has been developed building upon already-existing approaches: Water table fluctuations are estimated by introducing a groundwater reservoir below the soil layers (Yeh & Eltahir, 2005; Niu et al., 2007) and using specific yield to derive absolute groundwater levels (Lv et al., 2021; Healy & Cook, 2002). The groundwater flow is estimated by applying the linear reservoir assumption analogous to Lam et al. (2011); Sutanudjaja et al. (2018); Fenicia et al. (2006). The contribution of groundwater to evaporation is modelled by introducing a groundwater contribution fraction in the stress function of GLEAM; this fraction is defined as a function of soil moisture similar to Liu and Luo (2012).

Incorporating groundwater interactions increases the annual-mean, globally-averaged evaporation by 2.5 mm year^{-1}. The contribution of groundwater-sourced evaporation is estimated such that it is higher under dry conditions and for tall vegetation, in agreement with previous studies (Balugani et al., 2017; Miguez-Macho & Fan, 2021; Maxwell & Condon, 2016; Tfwala et al., 2021; Barbeta & Peñuelas, 2017). The globally-averaged contribution of groundwater to evaporation in GLEAM-Hydro ($f_{\mathrm{GW}} = 0.008$) is similar to findings by Miguez-Macho and Fan (2021), who estimate that approximately 1% of the global evaporation is sourced from groundwater. However, Barbeta and Peñuelas (2017) show a median $f_{\mathrm{GW}} = 0.56$ for tall vegetation in dry seasons which is almost twice as large compared to the findings of this study ($f_{\mathrm{GW}} = 0.31$, Fig. 7g). The spatial pattern of the groundwater contribution in this study differs considerably from previous studies (e.g. Miguez-Macho & Fan, 2021) and shows higher contributions in for example Canada, Russia and Congo where the groundwater levels are shallow (Fig. A8 in the Appendix). These differences may be attributed to uncertainties in the evaporation estimates in both this study (as discussed below) and previous studies.

There are several sources of uncertainty in the proposed approach to incorporate plant access to groundwater. First, this approach assumes lateral groundwater flow is insignificant at the chosen spatial resolution, which is plausible based on findings in previous studies (Krakauer et al., 2014). Second, this approach does not include capillary rise nor the existence of roots deeper than 2.5 m tapping into the groundwater system. Furthermore, we assume that there is no direct interaction between groundwater and the unsaturated zone (see also Section 2.1.4). These interactions are only mimicked through plants extracting (part of the) water from the groundwater, provided they have access to it, resulting in less extraction from the unsaturated zone and hence an increased soil moisture. That is also why the simulated soil moisture changes only marginally and the skill of soil moisture does not improve from GLEAM v3 to GLEAM-Hydro at the limited observation sites available (see Section 5.1.2). Moreover, results are sensitive to data uncertainties, including initial groundwater levels and soil properties. Last but not least, results here are constrained to the processes represented in GLEAM, which neglects human impacts such as pumping and irrigation. These are all potential avenues for improvements in the future, but are considered outside the scope of this study.

Alternatively, to reduce uncertainties related to the groundwater representation of GLEAM-Hydro, GLEAM could be coupled to a groundwater model. Its impact on the evaporation is illustrated for the Netherlands by using LHM-based groundwater levels as forcing in GLEAM (i.e., GLEAM-LHM). Compared to GLEAM-Hydro, GLEAM-LHM reproduces the spatial pattern of evaporation (Fig. A9 in the Appendix). However, the annual-mean evaporation for the region increases even more with GLEAM-LHM (4.8 mm year^{-1} or 0.2% relative to GLEAM v3) than with GLEAM-Hydro (2.4 mm year^{-1} or 0.1%). It is noted, however, that two-way coupling between evaporation and groundwater were not considered in GLEAM-LHM.

Future studies should address the limitations mentioned above. In addition, estimated groundwater level dynamics could be improved further by using total water storage anomalies as observed from satellites (Landerer & Swenson, 2012; Swenson & Wahr, 2006) for data assimilation. The proposed approach for groundwater–vegetation interactions could further be tested at higher resolutions. However, note that this may require additional modifications, since lateral groundwater flow may become significant at finer scales (de Graaf & Stahl, 2022). Furthermore, it would be very valuable if new eddy-covariance stations, located in dry regions and combined with groundwater level and root depth field observations, are available. This would benefit the verification of groundwater access and validation of evaporation at locations where groundwater becomes relevant. Unfortunately, most eddy-covariance stations used here are located in regions with deep water tables (according to Fan et al. (2013)) or in energy-limited regions with abundant water. As such, the effect of groundwater on evaporation could only be validated at a limited number of *in situ* stations.

7 Conclusion

The goal of this study was to incorporate plant access to groundwater in existing large-scale evaporation estimates, and to assess the impact of groundwater on evaporation globally. To that end, a novel, conceptual approach to estimate groundwater–vegetation interactions was developed. It connected conceptual elements of groundwater reservoirs and (observed) groundwater contributions to transpiration. This approach was incorporated into GLEAM, yielding the GLEAM-Hydro version of the model.

The impact of groundwater on evaporation was analysed globally by comparing GLEAM v3 with GLEAM-Hydro: While the globally-averaged annual-mean evaporation increased only by 2.5 mm year^{-1} (0.5%), local changes in regions with a shallow water table were much higher (up to 245.2 mm year^{-1}). In general, little improvements were found in the simulation of evaporation as the majority of the eddy-covariance stations was located in regions with no groundwater access or energy-limited regions, where the impact of groundwater on evaporation was marginal. However, at 75% of the stations where groundwater was a relevant water source, the temporal dynamics of the simulated evaporation improved. The skill of the model, also for other variables such as soil moisture and discharge, remained more or less unaltered. The skill of GLEAM-Hydro to simulate groundwater levels was further demonstrated through the comparison to a dedicated regional groundwater model (LHM). For the Netherlands, where abundant water table observations were available, both models showed considerable skill. However, LHM performed better in terms of $RMSE$ and KGE which was to be expected for a groundwater model calibrated for the Netherlands.

The presented approach paves the way towards the integration of groundwater in, for example, land surface and hydrological models and other algorithms that aim to derive evaporation from, for example, satellite-based observations. Representing groundwater in GLEAM also sets the ground to assimilate satellite gravimetry data in the future (Girotto et al., 2017). Even though the validation in this study could not unambiguously demonstrate the improved skill of the model, this approach is a first step towards a more realistic process representation in models that aim to incorporate groundwater processes at low computational costs.

Acknowledgement

This study was funded by the European Space Agency (ESA) through the projects DTE Hydrology Evolution (Contract no. ESA 4000136272/21/I-EF - CCN N. 1) and 4DMED-Hydrology (Contract no. ESA 4000136272/21/I-EF).

Data availability

All *in situ* observations were downloaded in June/July 2021 from multiple platforms as shown in Table A1. GLEAM output data that are generated in this study and are required to reproduce the main results and figures, are available at `https://doi.org/10.5281/zenodo.7099512`.

Appendix A

Table A1. *In situ* observations used in this study

Source	Long name	Data type	Nr stations	Website, Citation	Coverage
AmeriFlux	-	Radiation, meteorological & soil moisture data	512	https://ameriflux.lbl.gov/	Global
DINO	*Data en Informatie van de Nederlandse Ondergrond*	Groundwater level data	2750	https://www.dinoloket.nl/standen	The Netherlands
EFDC	European Fluxes Database Cluster	Radiation, meteorological & soil moisture data	88	http://www.europe-fluxdata.eu/	Global
FLUXNET-CH4	-	Radiation, meteorological & soil moisture data	67	https://fluxnet.org/, (Pastorello et al., 2020; Delwiche et al., 2021; Knox et al., 2019)	Global
GRDC	Global Runoff Data Centre	Discharge data	108	https://www.bafg.de/GRDC/EN/Home/homepage_node.html	Global
ICOS	Integrated Carbon Observation System	Radiation, meteorological & soil moisture data	145	https://www.icos-cp.eu/, (ICOS RI, 2021)	Global
IGRAC	International Groundwater Resources Assessment Centre	Groundwater level data	5359	https://ggis.un-igrac.org/view/ggmn	Global
ISMN	International Soil Moisture Network	Meteorological & soil moisture data	4672	https://ismn.geo.tuwien.ac.at/en/, (W. A. Dorigo et al., 2011; W. Dorigo et al., 2013, 2021)	Global

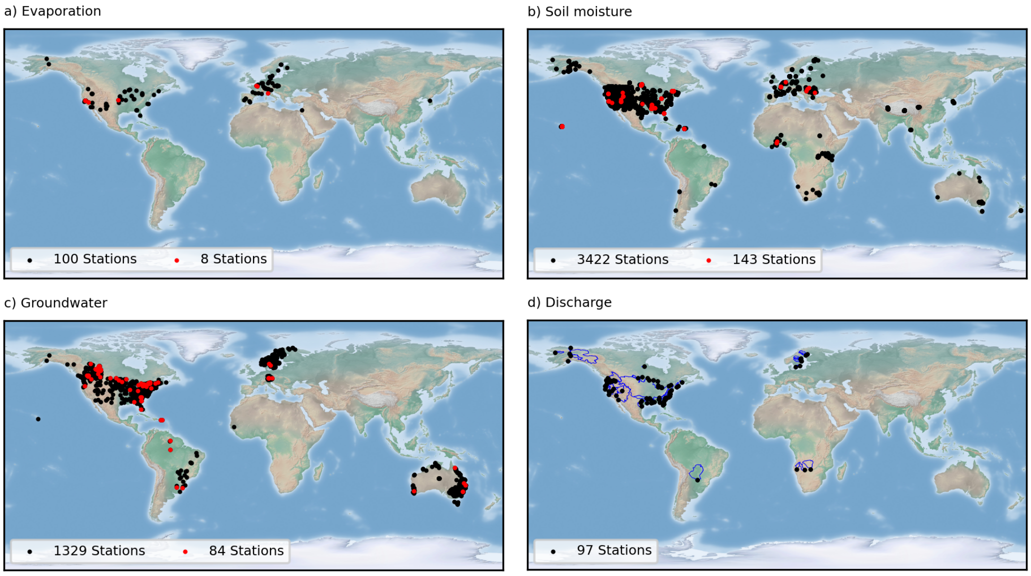

Figure A1. Map of stations with (a) evaporation, (b) soil moisture, (c) groundwater level, and (d) discharge stations (including basin outline in blue) used in this study. Black dots indicate all stations used, and red dots indicate stations where groundwater becomes a relevant source for evaporation.

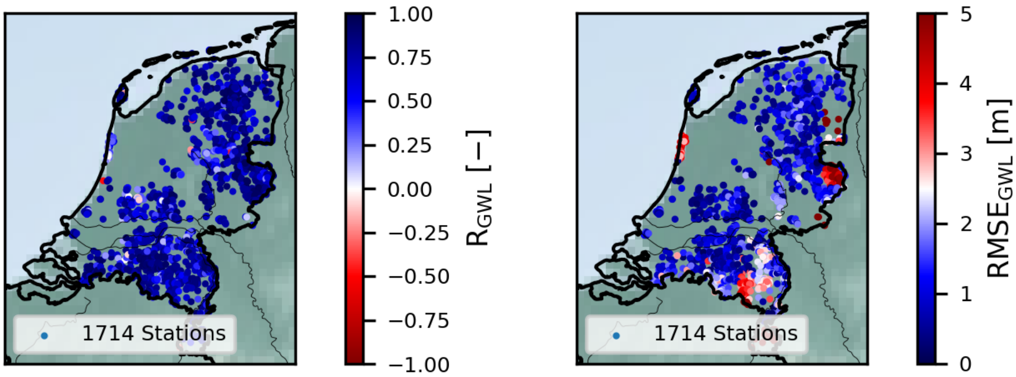

Figure A2. Groundwater level validation results in the Netherlands: a) correlation and b) *RMSE*

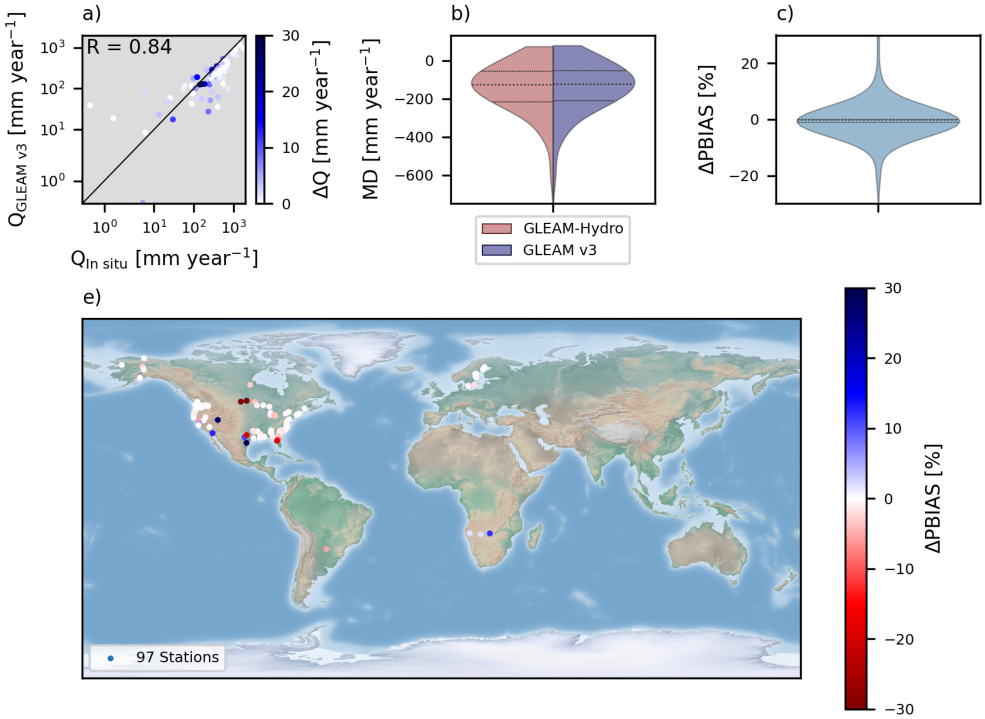

Figure A3. Runoff performance. a) Long-term average runoff according to *in situ* data (x-axis) vs. GLEAM v3 (y-axis) and with $\Delta Q_{\mathrm{GLEAM}} = Q_{\mathrm{GLEAMv3}} - Q_{\mathrm{GLEAM-Hydro}}$ for the colors. b) Mean difference (MD) for GLEAM v3 and GLEAM-Hydro with positive values indicating the GLEAM-based runoff are overestimated. c) Difference in $PBIAS$ (i.e., $\Delta PBIAS = PBIAS_{\mathrm{GLEAMv3}} - PBIAS_{\mathrm{GLEAM-Hydro}}$). d) Spatial pattern of $\Delta PBIAS$ with positive values indicating the bias improves in GLEAM-Hydro.

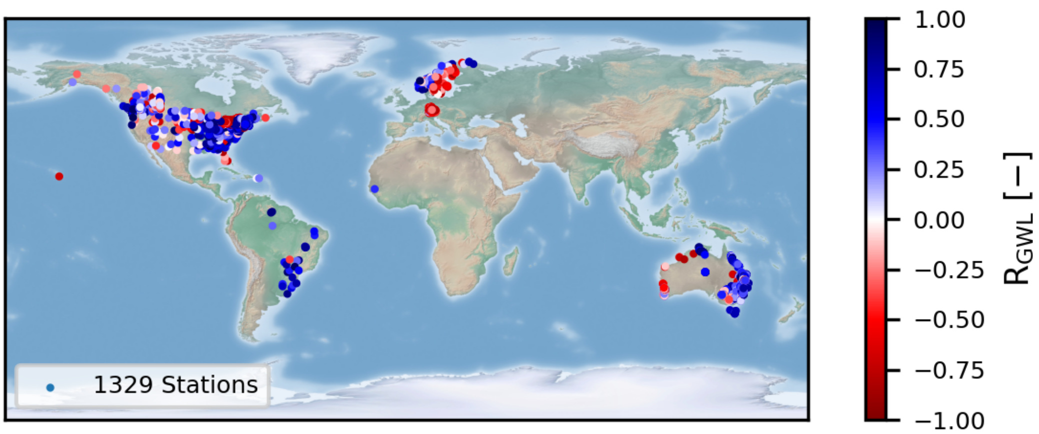

Figure A4. Global groundwater level validation results: Correlation

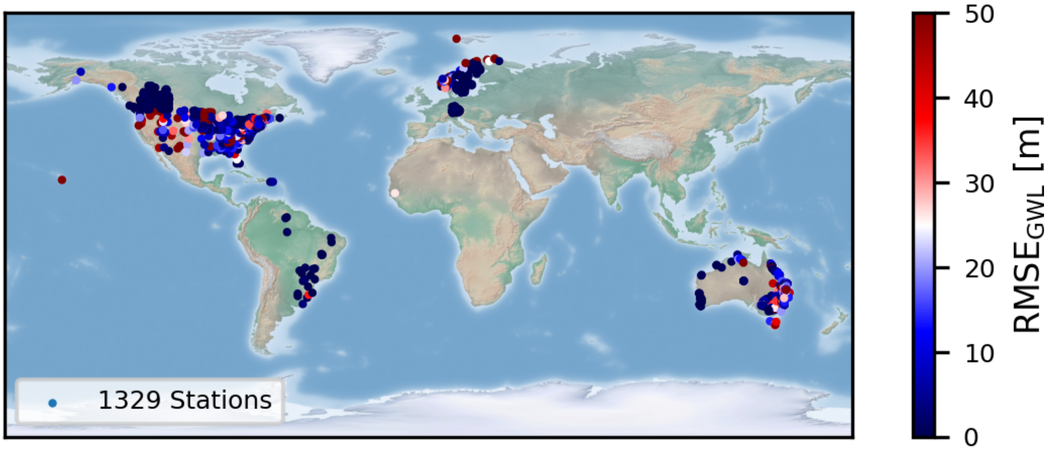

Figure A5. Global groundwater level validation results: $RMSE$

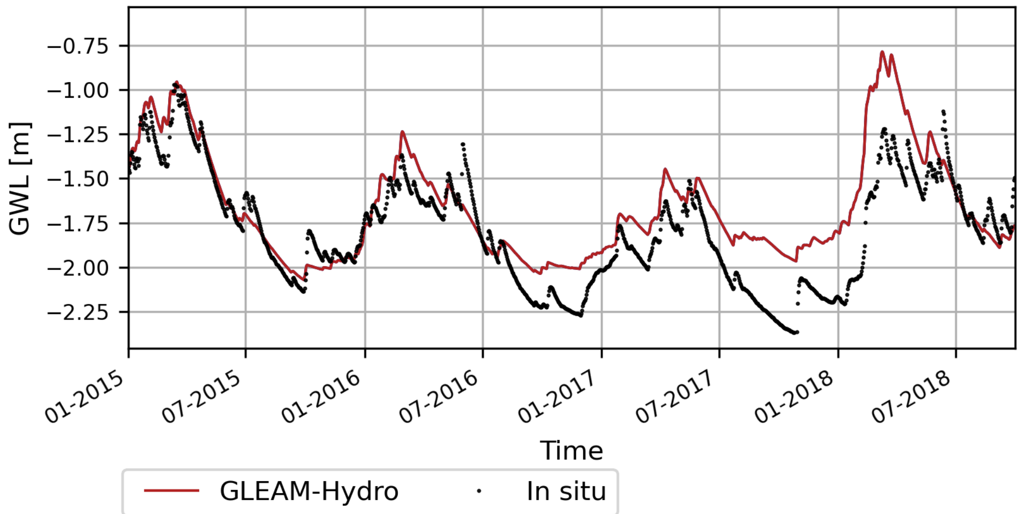

Figure A6. Groundwater levels at a well represented station near Philadelphia in the United States (74.84°W and 39.99°N).

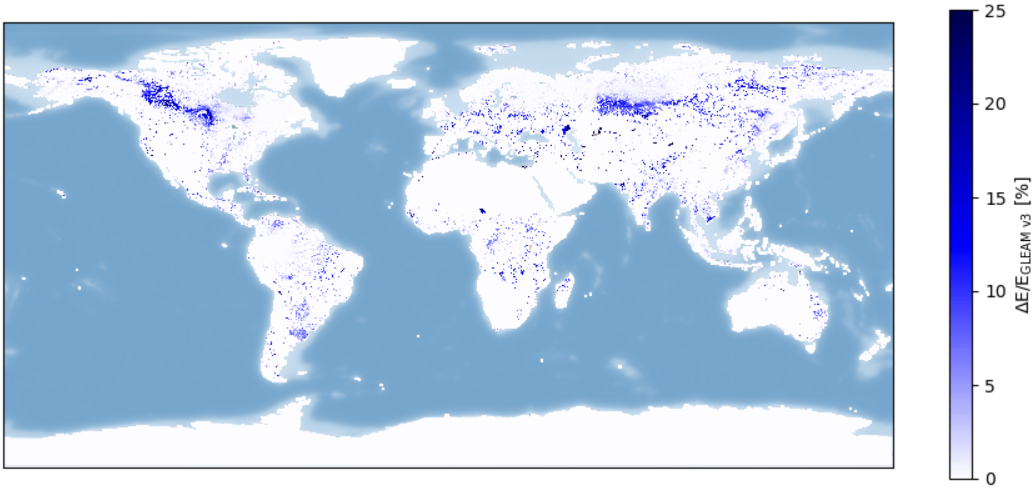

Figure A7. Average evaporation increase due to the incorporation of plant access to groundwater in GLEAM ($\Delta E = E_{\text{GLEAM-Hydro}} - E_{\text{GLEAMv3}}$) relative to GLEAM v3 averaged over the study period.

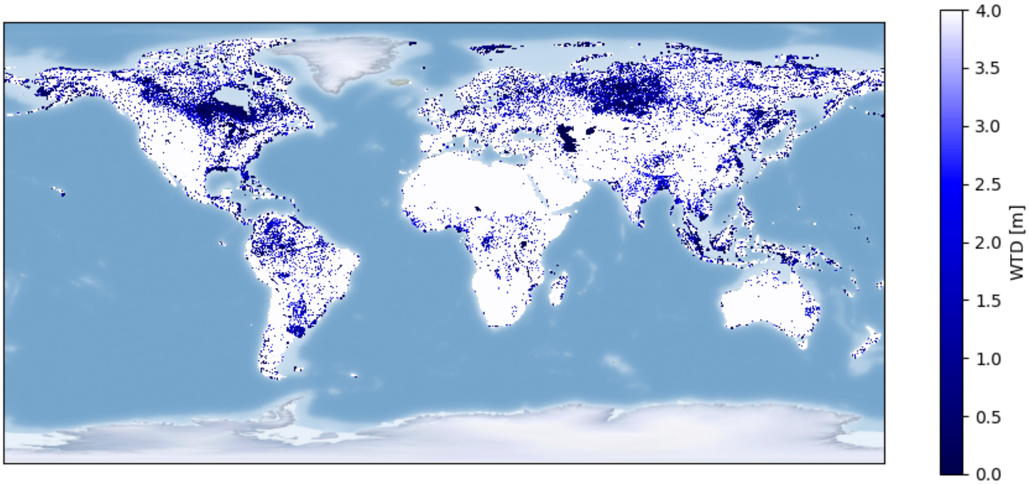

Figure A8. Initial groundwater level based on (Fan et al., 2013)

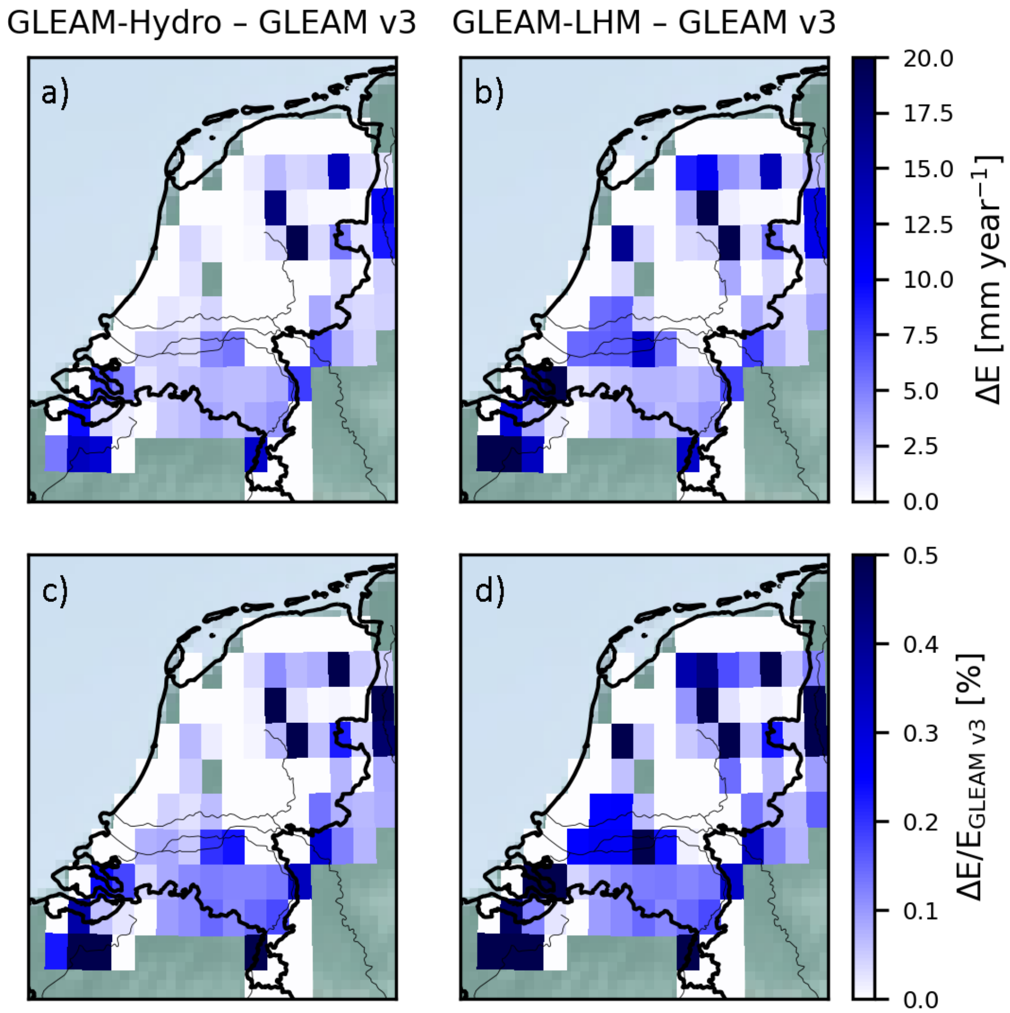

Figure A9. Average evaporation increase in the Netherlands due to the incorporation of plant access to groundwater in GLEAM. Subplots (a)–(b) illustrate absolute differences, subplots (c)–(d) relative differences. Suplots a) and c) use GLEAM-Hydro, subplots b) and d) use GLEAM-LHM. Absolute difference: $\Delta E = E_{\mathrm{GLEAM-Hydro/LHM}} - E_{\mathrm{GLEAMv3}}$, relative difference: $\frac{\Delta E}{E_{\mathrm{GLEAMv3}}}$

References

Amanambu, A. C., Obarein, O. A., Mossa, J., Li, L., Ayeni, S. S., Balogun, O., ... Ochege, F. U. (2020). Groundwater system and climate change: Present status and future considerations. *Journal of Hydrology*, *589*, 125163. Retrieved from `https://www.sciencedirect.com/science/article/pii/S0022169420306235` doi: https://doi.org/10.1016/j.jhydrol.2020.125163

Aumann, H., Chahine, M., Gautier, C., Goldberg, M., Kalnay, E., McMillin, L., ... Susskind, J. (2003). Airs/amsu/hsb on the aqua mission: design, science objectives, data products, and processing systems. *IEEE Transactions on Geoscience and Remote Sensing*, *41*(2), 253-264. doi: 10.1109/TGRS.2002.808356

Balugani, E., Lubczynski, M., Reyes-Acosta, L., van der Tol, C., Francés, A., & Metselaar, K. (2017). Groundwater and unsaturated zone evaporation and transpiration in a semi-arid open woodland. *Journal of Hydrology*, *547*, 54-66. doi: https://doi.org/10.1016/j.jhydrol.2017.01.042

Barbeta, A., & Peñuelas, J. (2017). Relative contribution of groundwater to plant transpiration estimated with stable isotopes. *Sci Rep*, *7*. doi: https://doi.org/10.1038/s41598-017-09643-x

Bastiaanssen, W., Menenti, M., Feddes, R., & Holtslag, A. (1998). A remote sensing surface energy balance algorithm for land (sebal). 1. formulation. *Journal of Hydrology*, *212-213*, 198-212. doi: https://doi.org/10.1016/S0022-1694(98)00253-4

Beck, H. E., Pan, M., Miralles, D. G., Reichle, R. H., Dorigo, W. A., Hahn, S., ... Wood, E. F. (2021). Evaluation of 18 satellite- and model-based soil moisture products using in situ measurements from 826 sensors. *Hydrology and Earth System Sciences*, *25*(1), 17–40. Retrieved from `https://hess.copernicus.org/articles/25/17/2021/` doi: 10.5194/hess-25-17-2021

Beck, H. E., Wood, E. F., Pan, M., Fisher, C. K., Miralles, D., van Dijk, A. I., ... Adler, R. F. (2019). MSWEP v2 global 3-hourly 0.1° precipitation : methodology and quantitative assessment. *BULLETIN OF THE AMERICAN METEOROLOGICAL SOCIETY*, *100*(3), 473–502. doi: https://doi.org/10.1175/BAMS-D-17-0138.1

Beyer, M., Hamutoko, J., Wanke, H., Gaj, M., & Koeniger, P. (2018). Examination of deep root water uptake using anomalies of soil water stable isotopes, depth-controlled isotopic labeling and mixing models. *Journal of Hydrology*, *566*, 122-136. doi: https://doi.org/10.1016/j.jhydrol.2018.08.060

Bieger, K., Arnold, J. G., Rathjens, H., White, M. J., Bosch, D. D., Allen, P. M., ... Srinivasan, R. (2017). Introduction to swat+, a completely restructured version of the soil and water assessment tool. *JAWRA Journal of the American Water Resources Association*, *53*(1), 115-130. doi: https://doi.org/10.1111/1752-1688.12482

Blyth, E. M., Arora, V. K., Clark, D. B., Dadson, S. J., De Kauwe, M. G., Lawrence, D. M., ... Yuan, H. (2021). Advances in land surface modelling. *Current Climate Change Reports*, *7*, 45–71. doi: https://doi.org/10.1007/s40641-021-00171-5

Clark, M. P., Fan, Y., Lawrence, D. M., Adam, J. C., Bolster, D., Gochis, D. J., ... Zeng, X. (2015). Improving the representation of hydrologic processes in earth system models. *Water Resources Research*, *51*(8), 5929-5956. doi: https://doi.org/10.1002/2015WR017096

Condon, L. E., Kollet, S., Bierkens, M. F. P., Fogg, G. E., Maxwell, R. M., Hill, M. C., ... Abesser, C. (2021). Global groundwater modeling and monitoring: Opportunities and challenges. *Water Resources Research*, *57*(12), e2020WR029500. Retrieved from `https://agupubs.onlinelibrary.wiley.com/doi/abs/10.1029/2020WR029500` doi: https://doi.org/10.1029/2020WR029500

de Graaf, I. E., van Beek, R. L., Gleeson, T., Moosdorf, N., Schmitz, O., Sutanudjaja, E. H., & Bierkens, M. F. (2017). A global-scale two-layer transient groundwater model: Development and application to groundwater depletion. *Advances in Water Resources*, *102*, 53-67. Retrieved from `https://www.sciencedirect.com/science/article/pii/S030917081630656X` doi: https://doi.org/10.1016/j.advwatres.2017.01.011

de Graaf, I., & Stahl, K. (2022). A model comparison assessing the importance of lateral groundwater flows at the global scale. *Environmental Research Letters*, *17*(4), 044020. doi: https://doi.org/10.1088/1748-9326/ac50d2

Delwiche, K. B., Knox, S. H., Malhotra, A., Fluet-Chouinard, E., McNicol, G., Feron, S., ... Jackson, R. B. (2021). Fluxnet-ch$_4$: a global, multi-ecosystem dataset and analysis of methane seasonality from freshwater wetlands. *Earth System Science Data*, *13*(7), 3607–3689. Retrieved from `https://essd.copernicus.org/articles/13/3607/2021/` doi: 10.5194/essd-13-3607-2021

DiMiceli, C., Carroll, M., Sohlberg, R., Kim, D., Kelly, M., & Townshend, J. (2015). *Mod44b modis/terra vegetation continuous fields yearly l3 global 250m sin grid v006 [data set].* NASA EOSDIS Land Processes DAAC. (Accessed on February 2022) doi: https://doi.org/10.5067/MODIS/MOD44B.006

Dorigo, W., Himmelbauer, I., Aberer, D., Schremmer, L., Petrakovic, I., Zappa, L., ... Sabia, R. (2021). The international soil moisture network: serving earth system science for over a decade. *Hydrology and Earth System Sciences*, *25*(11), 5749–5804. Retrieved from `https://hess.copernicus.org/articles/25/5749/2021/` doi: 10.5194/hess-25-5749-2021

Dorigo, W., Xaver, A., Vreugdenhil, M., Gruber, A., Hegyiová, A., Sanchis-Dufau, A., ... Drusch, M. (2013). Global automated quality control of in situ soil moisture data from the international soil moisture network. *Vadose Zone Journal*, *12*(3), vzj2012.0097. Retrieved from `https://acsess.onlinelibrary.wiley.com/doi/abs/10.2136/vzj2012.0097` doi: https://doi.org/10.2136/vzj2012.0097

Dorigo, W. A., Wagner, W., Hohensinn, R., Hahn, S., Paulik, C., Xaver, A., ... Jackson, T. (2011). The international soil moisture network: a data hosting facility for global in situ soil moisture measurements. *Hydrology and Earth System Sciences*, *15*(5), 1675–1698. Retrieved from `https://hess.copernicus.org/articles/15/1675/2011/` doi: 10.5194/hess-15-1675-2011

Evaristo, J., & McDonnell, J. J. (2017). Prevalence and magnitude of groundwater use by vegetation: a global stable isotope meta-analysis. *Scientific Reports*, *7*. doi: https://doi.org/10.1038/srep44110

Fan, Y. (2015). Groundwater in the earth's critical zone: Relevance to large-scale patterns and processes. *Water Resources Research*, *51*(5), 3052-3069. doi: https://doi.org/10.1002/2015WR017037

Fan, Y., Li, H., & Miguez-Macho, G. (2013). Global patterns of groundwater table depth. *Science*, *339*(6122), 940-943. doi: https://doi.org/10.1126/science.1229881

Fan, Y., Miguez-Macho, G., Jobbágy, E., Jackson, R., & Otero-Casal, C. (2017). Hydrologic regulation of plant rooting depth. *Proceedings of the National Academy of Sciences*, *114*(40), 10572-10577. doi: https://doi.org/10.1073/pnas.1712381114

Fenicia, F., Savenije, H. H. G., Matgen, P., & Pfister, L. (2006). Is the groundwater reservoir linear? learning from data in hydrological modelling. *Hydrology and Earth System Sciences*, *10*(1), 139–150. Retrieved from `https://hess.copernicus.org/articles/10/139/2006/` doi: 10.5194/hess-10-139-2006

Fisher, J. B., Melton, F., Middleton, E., Hain, C., Anderson, M., Allen, R., ... Wood, E. F. (2017). The future of evapotranspiration: Global requirements for ecosystem functioning, carbon and climate feedbacks, agricultural management, and water resources. *Water Resources Research*, *53*(4), 2618-2626. doi: https://doi.org/10.1002/2016WR020175

Fisher, J. B., Tu, K. P., & Baldocchi, D. D. (2008). Global estimates of the land–atmosphere water flux based on monthly avhrr and islscp-ii data, validated at 16 fluxnet sites. *Remote Sensing of Environment*, *112*(3), 901-919. Retrieved from `https://www.sciencedirect.com/science/article/pii/S0034425707003938` doi: https://doi.org/10.1016/j.rse.2007.06.025

Gao, H., Hrachowitz, M., Fenicia, F., Gharari, S., & Savenije, H. H. G. (2014). Testing the realism of a topography-driven model (flex-topo) in the nested catchments of the upper heihe, china. *Hydrology and Earth System Sciences*, *18*(5), 1895–1915. Retrieved from `https://hess.copernicus.org/articles/18/1895/2014/` doi: 10.5194/hess

-18-1895-2014

Girotto, M., De Lannoy, G. J. M., Reichle, R. H., Rodell, M., Draper, C., Bhanja, S. N., & Mukherjee, A. (2017). Benefits and pitfalls of grace data assimilation: A case study of terrestrial water storage depletion in india. *Geophysical Research Letters*, *44*(9), 4107-4115. Retrieved from https://agupubs.onlinelibrary.wiley.com/doi/abs/10.1002/2017GL072994 doi: https://doi.org/10.1002/2017GL072994

Gleeson, T., Wagener, T., Döll, P., Zipper, S. C., West, C., Wada, Y., ... Bierkens, M. F. P. (2021). Gmd perspective: The quest to improve the evaluation of groundwater representation in continental- to global-scale models. *Geoscientific Model Development*, *14*(12), 7545–7571. doi: https://doi.org/10.5194/gmd-14-7545-2021

Gupta, H. V., Kling, H., Yilmaz, K. K., & Martinez, G. F. (2009). Decomposition of the mean squared error and nse performance criteria: Implications for improving hydrological modelling. *Journal of Hydrology*, *377*(1), 80-91. Retrieved from https://www.sciencedirect.com/science/article/pii/S0022169409004843 doi: https://doi.org/10.1016/j.jhydrol.2009.08.003

Healy, R. W., & Cook, P. G. (2002). Using groundwater levels to estimate recharge. *Hydrogeology Journal*, *10*, 91 – 109. Retrieved from https://doi.org/10.1007/s10040-001-0178-0 doi: 10.1007/s10040-001-0178-0

ICOS RI. (2021). *Ecosystem final quality (l2) product in etc-archive format - release 2021-1 (version 1.0).* ICOS ERIC - Carbon Portal. doi: https://doi.org/10.18160/FZMY-PG92

Janssen, G., van Walsum, P., America, I., Pouwels, J., Hunink, J., Vermeulen, P., ... Kroon., T. (2020). *Veranderingsrapportage lhm 4.1: Beheer en onderhoud van de landelijke toepassing van het nhi.* Deltares rapport 11205261-000-BGS-0001. Retrieved from https://www.nhi.nu/nl/index.php/download_file/view/371/354/

Jung, M., Reichstein, M., & Bondeau, A. (2009). Towards global empirical upscaling of fluxnet eddy covariance observations: validation of a model tree ensemble approach using a biosphere model. *Biogeosciences*, *6*(10), 2001–2013. Retrieved from https://bg.copernicus.org/articles/6/2001/2009/ doi: https://doi.org/10.5194/bg-6-2001-2009

Kalma, J., McVicar, T., & McCabe, M. (2008). Estimating land surface evaporation: A review of methods using remotely sensed surface temperature data. *Surveys in Geophysics*, *29*, 421-469. doi: https://doi.org/10.1007/s10712-008-9037-z

Keune, J., Gasper, F., Goergen, K., Hense, A., Shrestha, P., Sulis, M., & Kollet, S. (2016). Studying the influence of groundwater representations on land surface-atmosphere feedbacks during the european heat wave in 2003. *Journal of Geophysical Research: Atmospheres*, *121*(22), 13,301-13,325. doi: https://doi.org/10.1002/2016JD025426

Knox, S. H., Jackson, R. B., Poulter, B., McNicol, G., Fluet-Chouinard, E., Zhang, Z., ... Zona, D. (2019). Fluxnet-ch_4 synthesis activity: Objectives, observations, and future directions. *Bulletin of the American Meteorological Society*, *100*(12), 2607–2632. doi: https://doi.org/10.1175/BAMS-D-18-0268.1

Kollet, S. J., & Maxwell, R. M. (2008). Capturing the influence of groundwater dynamics on land surface processes using an integrated, distributed watershed model. *Water Resources Research*, *44*(2). Retrieved from https://agupubs.onlinelibrary.wiley.com/doi/abs/10.1029/2007WR006004 doi: https://doi.org/10.1029/2007WR006004

Konapala, G., Mishra, A. K., Wada, Y., & Mann, M. E. (2020). Climate change will affect global water availability through compounding changes in seasonal precipitation and evaporation. *Nature Communications*, *11*(3044). doi: https://doi.org/10.1038/s41467-020-16757-w

Koppa, A., Alam, S., Miralles, D. G., & Gebremichael, M. (2021). Budyko-based long-term water and energy balance closure in global watersheds from earth observations. *Water Resources Research*, *57*(5), e2020WR028658. Retrieved from https://agupubs.onlinelibrary.wiley.com/doi/abs/10.1029/2020WR028658 (e2020WR028658 2020WR028658) doi: https://doi.org/10.1029/2020WR028658

Krakauer, N., Li, H., & Fan, Y. (2014, mar). Groundwater flow across spatial scales: importance for climate modeling. *Environmental Research Letters*, *9*(3), 034003. doi: https://doi.org/10.1088/1748-9326/9/3/034003

Kuffour, B. N. O., Engdahl, N. B., Woodward, C. S., Condon, L. E., Kollet, S., & Maxwell, R. M. (2020). Simulating coupled surface–subsurface flows with parflow v3.5.0: capabilities, applications, and ongoing development of an open-source, massively parallel, integrated hydrologic model. *Geoscientific Model Development*, *13*(3), 1373–1397. Retrieved from https://gmd.copernicus.org/articles/13/1373/2020/ doi: https://doi.org/10.5194/gmd-13-1373-2020

Laio, F., Tamea, S., Ridolfi, L., D'Odorico, P., & Rodriguez-Iturbe, I. (2009). Ecohydrology of groundwater-dependent ecosystems: 1. stochastic water table dynamics. *Water Resources Research*, *45*(5). Retrieved from https://agupubs.onlinelibrary.wiley.com/doi/abs/10.1029/2008WR007292 doi: https://doi.org/10.1029/2008WR007292

Lam, A., Karssenberg, D., van den Hurk, B. J. J. M., & Bierkens, M. F. P. (2011). Spatial and temporal connections in groundwater contribution to evaporation. *Hydrology and Earth System Sciences*, *15*(8), 2621–2630. Retrieved from https://hess.copernicus.org/articles/15/2621/2011/ doi: 10.5194/hess-15-2621-2011

Landerer, F. W., & Swenson, S. C. (2012). Accuracy of scaled grace terrestrial water storage estimates. *Water Resources Research*, *48*(4). Retrieved from https://agupubs.onlinelibrary.wiley.com/doi/abs/10.1029/2011WR011453 doi: https://doi.org/10.1029/2011WR011453

Langevin, C., Hughes, J., Banta, E., Provost, A., Niswonger, R., & Panday, S. (2017). *Modflow 6 modular hydrologic model: U.s. geological survey software.* doi: https://doi.org/10.5066/F76Q1VQV

Liu, T., Liu, L., Luo, Y., & Lai, J. (2015). Simulation of groundwater evaporation and groundwater depth using swat in the irrigation district with shallow water table. *Environmental Earth Sciences*, *74*(1), 315-324. doi: 10.1007/s12665-015-4034-2

Liu, T., & Luo, Y. (2012). An empirical approach simulating evapotranspiration from groundwater under different soil water conditions. *Environmental Earth Sciences*, *67*(5), 1345-1355. doi: 10.1007/s12665-012-1577-3

Loew, A., Peng, J., & Borsche, M. (2016). High-resolution land surface fluxes from satellite and reanalysis data (holaps v1.0): evaluation and uncertainty assessment. *Geoscientific Model Development*, *9*(7), 2499–2532. Retrieved from https://gmd.copernicus.org/articles/9/2499/2016/ doi: 10.5194/gmd-9-2499-2016

Lv, M., Xu, Z., Yang, Z.-L., Lu, H., & Lv, M. (2021). A comprehensive review of specific yield in land surface and groundwater studies. *Journal of Advances in Modeling Earth Systems*, *13*(2), e2020MS002270. Retrieved from https://agupubs.onlinelibrary.wiley.com/doi/abs/10.1029/2020MS002270 doi: https://doi.org/10.1029/2020MS002270

Mallick, K., Jarvis, A. J., Boegh, E., Fisher, J. B., Drewry, D. T., Tu, K. P., ... Niyogi, D. (2014). A surface temperature initiated closure (stic) for surface energy balance fluxes. *Remote Sensing of Environment*, *141*, 243-261. Retrieved from https://www.sciencedirect.com/science/article/pii/S0034425713003908 doi: https://doi.org/10.1016/j.rse.2013.10.022

Martens, B., Miralles, D. G., Lievens, H., van der Schalie, R., de Jeu, R. A. M., Fernández-Prieto, D., ... Verhoest, N. E. C. (2017). Gleam v3: satellite-based land evaporation and root-zone soil moisture. *Geoscientific Model Development*, *10*(5), 1903–1925. Retrieved from https://gmd.copernicus.org/articles/10/1903/2017/ doi: 10.5194/gmd-10-1903-2017

Martens, B., Schumacher, D. L., Wouters, H., Muñoz Sabater, J., Verhoest, N. E. C., & Miralles, D. G. (2020). Evaluating the land-surface energy partitioning in era5. *Geoscientific Model Development*, *13*(9), 4159–4181. Retrieved from https://gmd.copernicus.org/articles/13/4159/2020/ doi: 10.5194/gmd-13-4159-2020

Maxwell, R., & Condon, L. (2016). Connections between groundwater flow and transpiration partitioning. *Science*, *353*(6297), 377-380. doi: 10.1126/science.aaf7891

Maxwell, R., & Miller, N. (2005). Development of a coupled land surface and groundwater model. *Journal of Hydrometeorology*, *6*(3), 233 – 247. doi: https://doi.org/10.1175/JHM422.1

Miguez-Macho, G., & Fan, Y. (2021). Spatiotemporal origin of soil water taken up by vegetation. *Nature*, *598*, 624–628. doi: https://doi.org/10.1038/s41586-021-03958-6

Miralles, D. G., Holmes, T. R. H., De Jeu, R. A. M., Gash, J. H., Meesters, A. G. C. A., & Dolman, A. J. (2011). Global land-surface evaporation estimated from satellite-based observations. *Hydrology and Earth System Sciences*, *15*(2), 453–469. Retrieved from https://hess.copernicus.org/articles/15/453/2011/ doi: https://doi.org/10.5194/hess-15-453-2011

Moesinger, L., Dorigo, W., de Jeu, R., van der Schalie, R., Scanlon, T., Teubner, I., & Forkel, M. (2020). The global long-term microwave vegetation optical depth climate archive (vodca). *Earth System Science Data*, *12*(1), 177–196. Retrieved from https://essd.copernicus.org/articles/12/177/2020/ doi: 10.5194/essd-12-177-2020

Niu, G.-Y., Yang, Z.-L., Dickinson, R. E., Gulden, L. E., & Su, H. (2007). Development of a simple groundwater model for use in climate models and evaluation with gravity recovery and climate experiment data. *Journal of Geophysical Research: Atmospheres*, *112*(D7). Retrieved from https://agupubs.onlinelibrary.wiley.com/doi/abs/10.1029/2006JD007522 doi: https://doi.org/10.1029/2006JD007522

Oki, T., & Kanae, S. (2006). Global hydrological cycles and world water resources. *Science*, *313*(5790), 1068-1072. doi: https://doi.org/10.1126/science.1128845

Orellana, F., Verma, P., Loheide II, S. P., & Daly, E. (2012). Monitoring and modeling water-vegetation interactions in groundwater-dependent ecosystems. *Reviews of Geophysics*, *50*(3). doi: https://doi.org/10.1029/2011RG000383

Pastorello, G., Trotta, C., Canfora, E., Chu, H., Christianson, D., Cheah, Y.-W., ... Papale, D. (2020, 7 9). The fluxnet2015 dataset and the oneflux processing pipeline for eddy covariance data. *Scientific Data*, *7*(1). doi: 10.1038/s41597-020-0534-3

Priestley, C. H. B., & Taylor, R. J. (1972). On the assessment of surface heat flux and evaporation using large-scale parameters. *Monthly Weather Review*, *100*(2), 81 - 92. Retrieved from https://journals.ametsoc.org/view/journals/mwre/100/2/1520-0493_1972_100_0081_otaosh_2_3_co_2.xml doi: 10.1175/1520-0493(1972)100⟨0081:OTAOSH⟩2.3.CO;2

Samaniego, L., Kumar, R., & Attinger, S. (2010). Multiscale parameter regionalization of a grid-based hydrologic model at the mesoscale. *Water Resources Research*, *46*(5). doi: https://doi.org/10.1029/2008WR007327

Su, Z. (2002). The surface energy balance system (sebs) for estimation of turbulent heat fluxes. *Hydrology and Earth System Sciences*, *6*(1), 85–100. doi: https://doi.org/10.5194/hess-6-85-2002

Sulis, M., Couvreur, V., Keune, J., Cai, G., Trebs, I., Junk, J., ... others (2019). Incorporating a root water uptake model based on the hydraulic architecture approach in terrestrial systems simulations. *Agricultural and Forest Meteorology*, *269*, 28–45. Retrieved from https://www.sciencedirect.com/science/article/pii/S0168192319300437 doi: https://doi.org/10.1016/j.agrformet.2019.01.034

Sulis, M., Williams, J., Shrestha, P., Diederich, M., Simmer, C., Kollet, S., & Maxwell, R. (2017). Coupling groundwater, vegetation, and atmospheric processes: A comparison of two integrated models. *Journal of Hydrometeorology*, *18*(5), 1489 – 1511. doi: https://doi.org/10.1175/JHM-D-16-0159.1

Sutanudjaja, E. H., van Beek, R., Wanders, N., Wada, Y., Bosmans, J. H. C., Drost, N., ... Bierkens, M. F. P. (2018). PCR-GLOBWB 2: a 5 arcmin global hydrological and water resources model. *Geoscientific Model Development*, *11*(6), 2429–2453. doi: https://doi.org/10.5194/gmd-11-2429-2018

Swenson, S., & Wahr, J. (2006). Post-processing removal of correlated errors in grace data. *Geophysical Research Letters*, *33*(8). Retrieved from https://agupubs.onlinelibrary.wiley.com/doi/abs/10.1029/2005GL025285 doi: https://doi

.org/10.1029/2005GL025285

Takala, M., Luojus, K., Pulliainen, J., Derksen, C., Lemmetyinen, J., Kärnä, J.-P., … Bojkov, B. (2011). Estimating northern hemisphere snow water equivalent for climate research through assimilation of space-borne radiometer data and ground-based measurements. *Remote Sensing of Environment*, *115*(12), 3517-3529. Retrieved from https://www.sciencedirect.com/science/article/pii/S0034425711003166 doi: https://doi.org/10.1016/j.rse.2011.08.014

Taylor, R. G., Scanlon, B., Döll, P., Rodell, M., van Beek, R., Wada, Y., … Treidel, H. (2013). Ground water and climate change. *Nature Climate Change*, *3*, 322–329. Retrieved from https://doi.org/10.1038/nclimate1744 doi: 10.1038/nclimate1744

Tfwala, C., van Rensburg, L., & Bello, Z. (2021). Groundwater contribution to transpiration of trees under wet and dry soil conditions. *Irrigation and Drainage*, *70*(1), 42-51. doi: https://doi.org/10.1002/ird.2533

Tian, W., Li, X., Cheng, G.-D., Wang, X.-S., & Hu, B. X. (2012). Coupling a groundwater model with a land surface model to improve water and energy cycle simulation. *Hydrology and Earth System Sciences*, *16*(12), 4707–4723. Retrieved from https://hess.copernicus.org/articles/16/4707/2012/ doi: https://doi.org/10.5194/hess-16-4707-2012

Trenberth, K., Fasullo, J., & Kiehl, J. (2009). Earth's global energy budget. *American Meteorological Society*(90), 311–323. doi: https://doi.org/10.1175/2008BAMS2634.1

Trenberth, K. E., Smith, L., Qian, T., Dai, A., & Fasullo, J. (2007). Estimates of the global water budget and its annual cycle using observational and model data. *Journal of Hydrometeorology*, *8*(4), 758–769. doi: https://doi.org/10.1175/JHM600.1

van der Ent, R. J., Savenije, H. H. G., Schaefli, B., & Steele-Dunne, S. C. (2010). Origin and fate of atmospheric moisture over continents. *Water Resources Research*, *46*(9). Retrieved from https://agupubs.onlinelibrary.wiley.com/doi/abs/10.1029/2010WR009127 doi: https://doi.org/10.1029/2010WR009127

Vicente-Serrano, S. M., Beguería, S., & López-Moreno, J. I. (2010). A multiscalar drought index sensitive to global warming: The standardized precipitation evapotranspiration index. *Journal of Climate*, *23*(7), 1696 - 1718. Retrieved from https://journals.ametsoc.org/view/journals/clim/23/7/2009jcli2909.1.xml doi: 10.1175/2009JCLI2909.1

Wielicki, B. A., Barkstrom, B. R., Harrison, E. F., Lee, R. B., Smith, G. L., & Cooper, J. E. (1996). Clouds and the earth's radiant energy system (ceres): An earth observing system experiment. *Bulletin of the American Meteorological Society*, *77*(5), 853 - 868. Retrieved from https://journals.ametsoc.org/view/journals/bams/77/5/1520-0477_1996_077_0853_catere_2_0_co_2.xml doi: 10.1175/1520-0477(1996)077⟨0853:CATERE⟩2.0.CO;2

Yeh, P.-F., & Eltahir, E. (2005). Representation of water table dynamics in a land surface scheme. part i: Model development. *Journal of Climate*, *18*(12), 1861-1880. doi: 10.1175/JCLI3330.1

Zhang, J., Bai, Y., Yan, H., Guo, H., Yang, S., & Wang, J. (2020). Linking observation, modelling and satellite-based estimation of global land evapotranspiration. *Big Earth Data*, *4*(2), 94-127. doi: https://doi.org/10.1080/20964471.2020.1743612

Zhang, K., Kimball, J. S., & Running, S. W. (2016). A review of remote sensing based actual evapotranspiration estimation. *WIREs Water*, *3*(6), 834-853. doi: https://doi.org/10.1002/wat2.1168